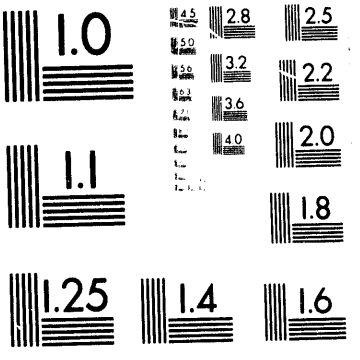
1.0
1.1
1.25
1.4
1.6
1.8
2.0
2.2
2.5
2.8
3.2
3.6
4.0
4.5
5.0
5.6
6.3

1 of 1

2

DOE/MC/26288-3609

MTCI 10038-17

TECHNICAL PROGRESS REPORT

July 1993 - September 1993

For:

U.S. Department of Energy
Morgantown Energy Technology Center

Under:

DOE Contract No. DE-AC21-89MC26288

Sonic Enhanced Ash Agglomeration and Sulfur Capture

By:

MANUFACTURING AND TECHNOLOGY CONVERSION INTERNATIONAL, INC.
P.O. Box 21, Columbia, Maryland 21045-0021

PREFACE

This 17th Quarterly Technical Progress Report presents the results of work accomplished during the period June 28, 1993 through September 26, 1993 under Contract No. DE-AC21-88MC26288 entitled "Sonic Enhanced Ash Agglomeration and Sulfur Capture." The fundamental studies conducted by West Virginia University and Penn State University are provided in Subsections 2.2 and 2.3.

The system modifications for continuous feed and long duration testing were completed. Several modifications to the existing PAFBC system were made so that the calcination of sorbents for the test program can be readily accomplished.

West Virginia University has completed the Analysis and Design techniques for determining aerovalve geometry and performance and initiated work on design optimization prior to the fabrication and testing of an aerovalve for verification of the design analysis.

PSU - The modifications to the Entrained Flow Reactor, EFR, were completed and calcination tests to determine the effect of size on the rate and temperature of calcination without acoustics were completed and showed a significant increase in sorbent surface area and pore volume with the extent of calcination. A series of test runs were also conducted in the EFR to measure particle concentrations and size distributions of ash with and without an acoustic field.

TABLE OF CONTENTS

LIST OF FIGURES

LIST OF FIGURES
(CONT'D)

LIST OF FIGURES
(CONT'D)

LIST OF TABLES

SECTION 1.0

INTRODUCTION

1.1 PROJECT DESCRIPTION AND WORK STATUS

A major concern with the utilization of coal in directly fired gas turbines is the control of particulate emissions and reduction of sulfur dioxide, and alkali vapor from combustion of coal, upstream of the gas turbine. Much research and development has been sponsored on methods for particulate emissions control and the direct injection of calcium-based sorbents to reduce SO_2 emission levels. The results of this research and development indicate that both acoustic agglomeration of particulates and direct injection of sorbents have the potential to become a significant emissions control strategy.

The Sonic Enhanced Ash Agglomeration and Sulfur Capture program focuses upon the application of an MTCI proprietary invention (Patent No. 5,197,399) for simultaneously enhancing sulfur capture and particulate agglomeration of the combustor effluent. This application can be adapted as either a "hot flue gas cleanup" subsystem for the current concepts for combustor islands or as an alternative primary pulse combustor island in which slagging, sulfur capture, particulate agglomeration and control, and alkali gettering as well as NO_x control processes become an integral part of the pulse combustion process.

The goal of the program is to support the DOE mission in developing coal-fired combustion gas turbines. In particular, the MTCI proprietary process for bimodal ash agglomeration and simultaneous sulfur capture will be evaluated and developed. The technology embodiment of the invention provides for the use of standard grind, moderately beneficiated coal and WEM for firing the gas turbine with efficient sulfur capture and particulate emission control upstream of the turbine. The process also accommodates injection of alkali gettering material if necessary. This is aimed at utilization of relatively inexpensive coal fuels, thus realizing the primary benefit being sought by direct firing of coal in such gas turbine systems. The proposed technology provides for practical, reliable,

and capital (and O&M) cost-effective means of protection for the gas turbine from impurities in the coal combustor effluent.

1.2 PROGRAM OBJECTIVES

The major objective of the Phase I test program is to confirm the feasibility of the MTCI bimodal particle size approach to enhance particulate control by acoustic ash agglomeration. An ancillary objective of the Phase I effort is to demonstrate and confirm the feasibility of an acoustic field to enhance sulfur capture by increasing sorbent reactivity. Phase I tests are designed to cover the frequency range between 50 and 1400 Hz, establish monomodal baseline performance as a benchmark from which to measure the degree of enhancement expected from the bimodal approach, and, finally, to confirm the effectiveness of low-frequency fields over high-frequency fields for realistic particulate streams.

The program will demonstrate the effectiveness of a unique approach which uses a bimodal distribution composed of large sorbent particles and fine fly ash particles to enhance ash agglomeration and sulfur capture at conditions found in direct coal-fired turbines. Under the impact of high-intensity sound waves, sorbent reactivity and utilization, it is theorized, will increase while agglomerates of fly ash and sorbents are formed which are readily collected in commercial cyclones. The work will extend the concept from the demonstration of feasibility (Phase I), through proof-of-concept (Phase II) to the construction (Phase III) of a coal-fired pulsed combustor with in-furnace sorbent injection. For Phase I, Pennsylvania State University will conduct studies for enhanced sulfur capture in The Combustion Laboratory and agglomeration tests in the High Intensity Acoustic Laboratory.

1.3 SUMMARY STATUS FOR THE PERIOD

The system modifications for continuous feed and long duration testing were completed. Several modifications to the existing PAFBC system were made so that the calcination of sorbents for the test program can be readily accomplished.

West Virginia University has completed the Analysis and Design techniques for determining aerovalve geometry and performance and initiated work on design

optimization prior to the fabrication and testing of an aerovalve for verification of the design analysis.

PSU - The modifications to the Entrained Flow Reactor, EFR, were completed and calcination tests to determine the effect of size on the rate and temperature of calcination without acoustics were completed. The data was consistent with previous studies that show a significant increase in sorbent surface area and pore volume with the extent of calcination. A series of test runs were also conducted in the EFR to measure particle concentrations and size distributions of ash with and without an acoustic field.

The sulfation model was used to simulate sulfation of carbonate and calcium hydroxide particles. The results of the simulation will be compared with the experimental observations during the next period.

SECTION 2.0

TECHNICAL DISCUSSION OF THE WORK ACCOMPLISHED DURING THE REPORTING PERIOD

2.1 TASK 1: SHAKEDOWN TESTING

SCREENING TESTS

The sorbent feed system was modified for continuous feed and long duration testing (see Figures 1 and 2). The system consists of a K-Tron screw feeder installed inside the primary injector vessel, a storage injector installed above the primary injector vessel, and a sorbent loading cone above the storage injector. There are two ball valves in the loading line: one at the bottom (V1) and one at the top (V2) of the storage injector. The primary injector vessel is under pressure all the time during the test and the screw feeder is running. Valve V1 is closed and valve V2 is open. Sorbent from the loading cone drops into the storage injector vessel. When the sorbent level in the feeder inside the primary injector vessel is low, the level sensor sends a signal about the low level of sorbent. At that time, valve V2 on the top of the storage injector is closed and the vessel is pressurized to equalize the pressure with primary injector vessel pressure. Then, valve V1 is opened and sorbent drops from the storage vessel to the feeder hopper inside the primary injector vessel. Valve V1 is then closed and the storage vessel is depressurized through a denim bag. After depressurization, ball valve V2 is opened and sorbent is fed through a loading cone into the storage vessel. This process is repeated to maintain sorbent level in the primary injector and to enable continuous feed of sorbent.

It was found during our tests that solids (agglomerated ash and sorbent) accumulated on the reflection cone in the agglomeration chamber, overfilled it, and dropped onto the bottom flange of the agglomeration chamber. The included angle of the existing reflection cone is 120° and is greater than that required based on solids repose angle. It was therefore decided to replace this cone with a 60° angle reflection cone and install above it a collection cone that will overlap with the reflection cone to prevent solids bypass to the bottom of the

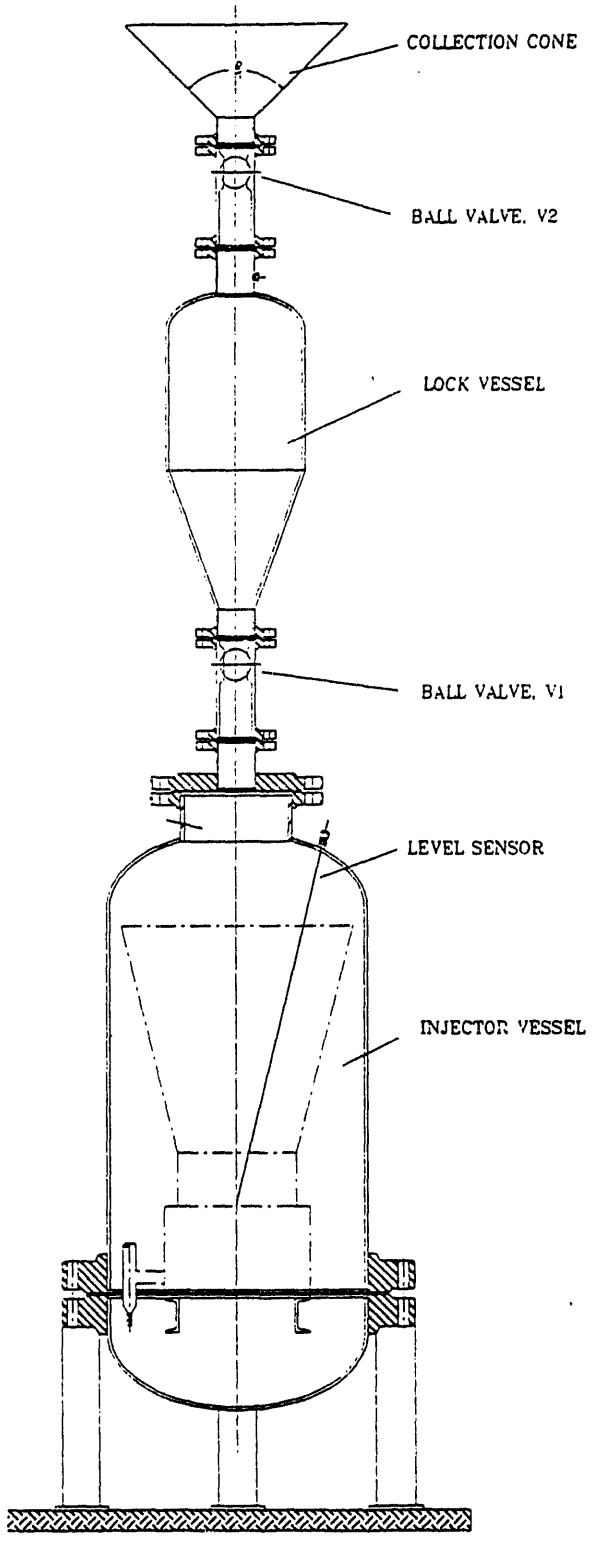

FIGURE 1: SORBENT FEEDER FOR CONTINUOUS FEEDING APPLICATION

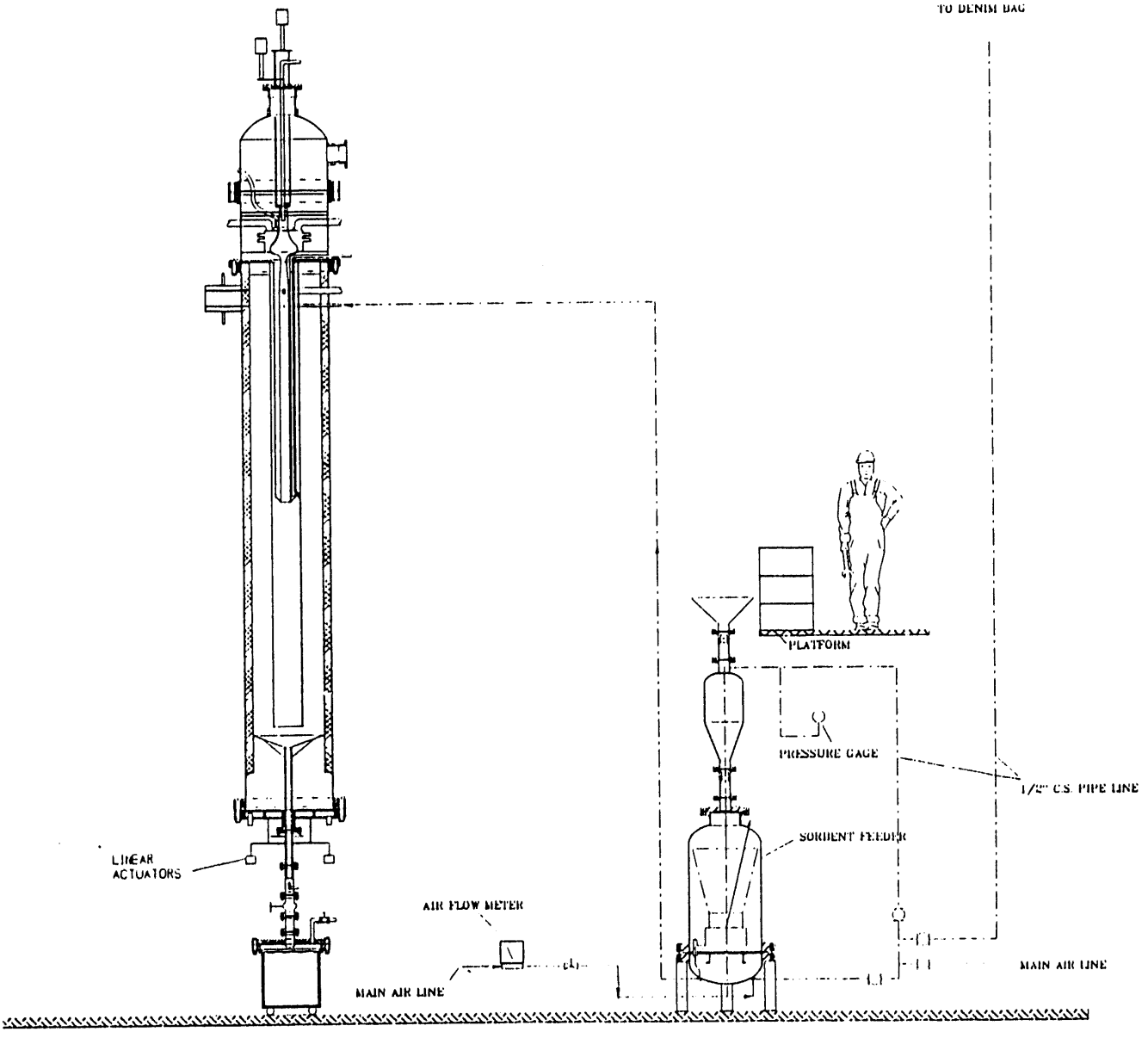

FIGURE 2: P&ID OF CONTINUOUS SORBENT FEED

agglomeration chamber (see Figure 3). It was also found during inspection of the agglomeration chamber catch section that the 2-inch solids drain pipe has a dent and caused flow obstruction. Unlike the original reflection shield which was designed to traverse/telescope, the new cone is not required to be mobile. Therefore, to facilitate improved solids flow into the catch pot and provide pressure seal, it was also decided to replace the existing drain line by a 3-inch line with one pressure sealing union. The vacuum pump had difficulty providing suction at high velocity to generate an isokinetic sample over a significant time interval (20 to 30 minutes). This was attributed to the 3-inch line downstream of the pressure letdown valve and pump operating characteristics and limitations including overheating. To reduce solids loading and increase isokinetic sampling duration and reliability, it was decided to replace the 3-inch pipe with a 6-inch pipe and substitute an eductor arrangement for the vacuum pump.

The reflection cone was installed on the drain pipe and a collection conical ring was welded to the wall of the chamber. The drain line now comprises a 3-inch pipe with one pressure sealing union (Figure 4) for inspection purposes and to vacuum out any solids which collect during the test to verify mass balance.

For calcination and classification of the sorbents, it was decided to use the existing PAFBC pulse combustor facility (see Figure 5). Sorbent will be fed into the pulse combustion chamber fired with natural gas. The pulse combustor will be maintained in the 1800 - 2000°F temperature range and the very shallow (2 - 6" bed depth) fluidized bed and freeboard in the 1500 to 1600°F range to maximize calcination and minimize sintering. Big size particulates will be accumulated in the bed and will be drained. Classified lime (preferably box 10 microns) will be collected in the cyclone catch and will be used later as sorbent in the bimodal tests. The PAFBC pulse combustor needs some repair work. It will be taken off the facility, repaired and re-installed. After preparation of classified lime, the bimodal tests will be continued.

The MTCI PAFBC system underwent some repair work in preparation for sorbent calcination and classification. The bed was drained and the bed door was opened. Damaged refractory on the door was removed and new refractory was cast and cured. The bed area and freeboard burners and their controls were inspected and tested.

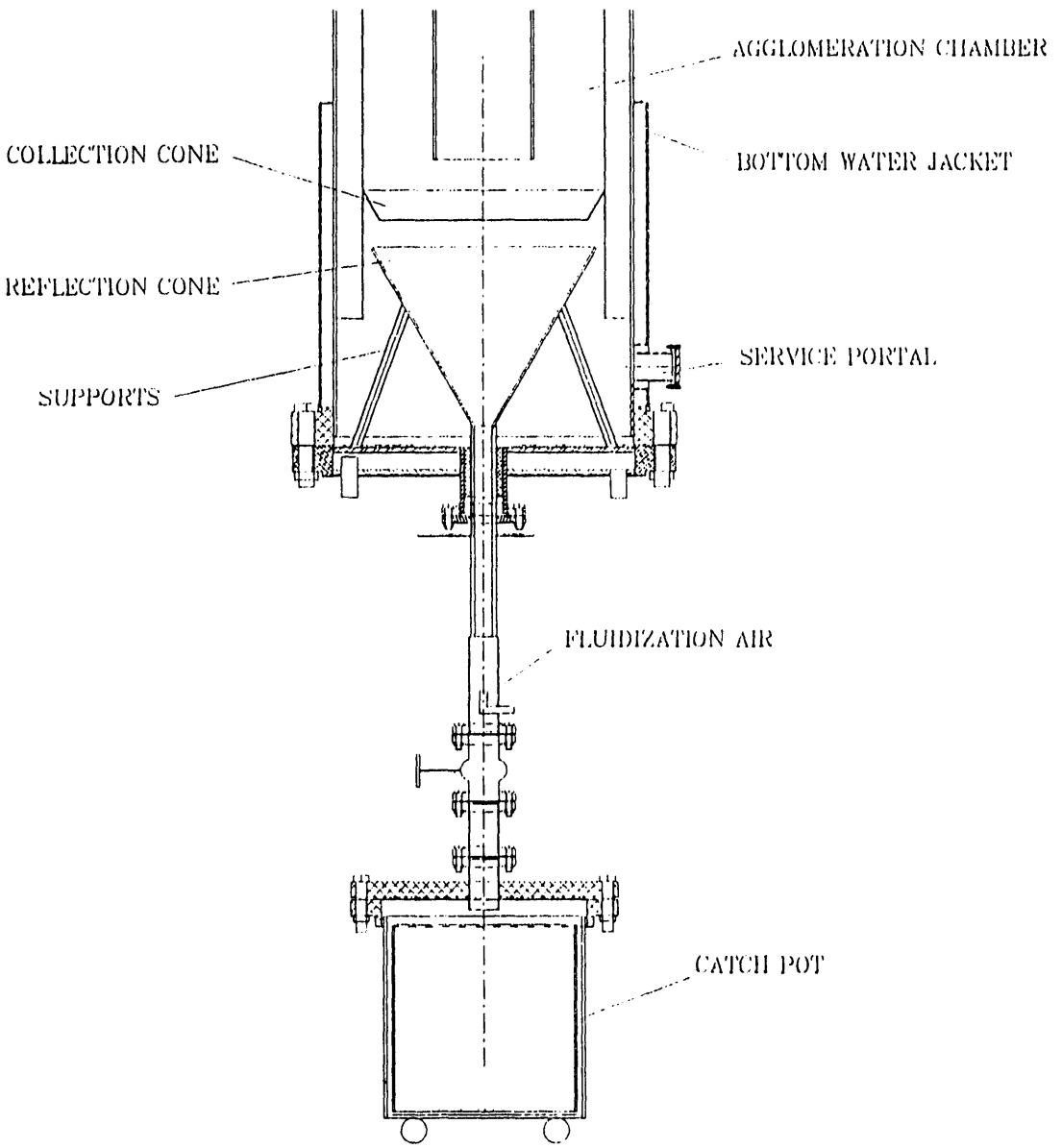

FIGURE 3: MODIFICATION OF REFLECTION CONE

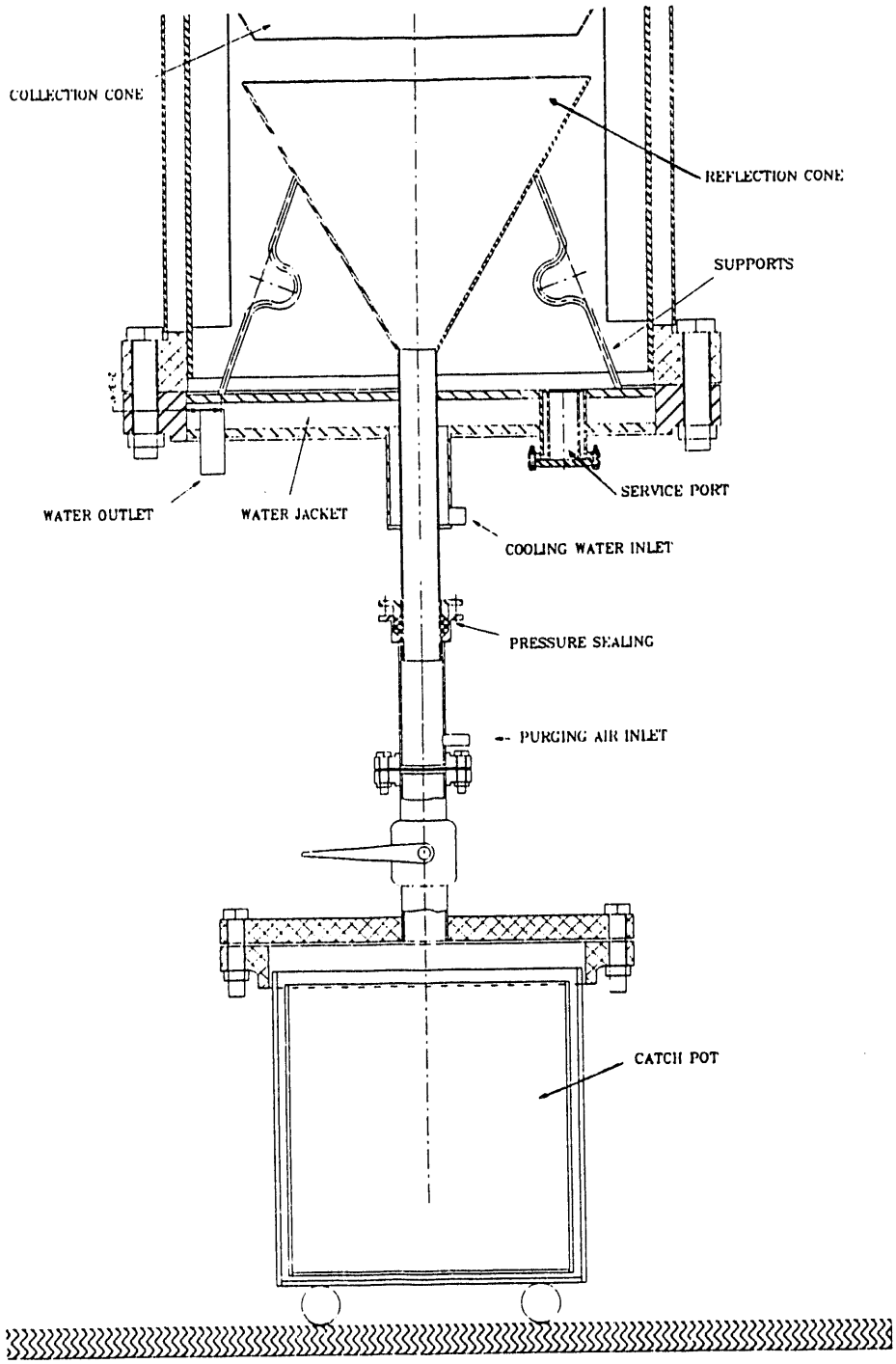

FIGURE 4: MODIFIED AGGLOMERATION CHAMBER BOTTOM SECTION

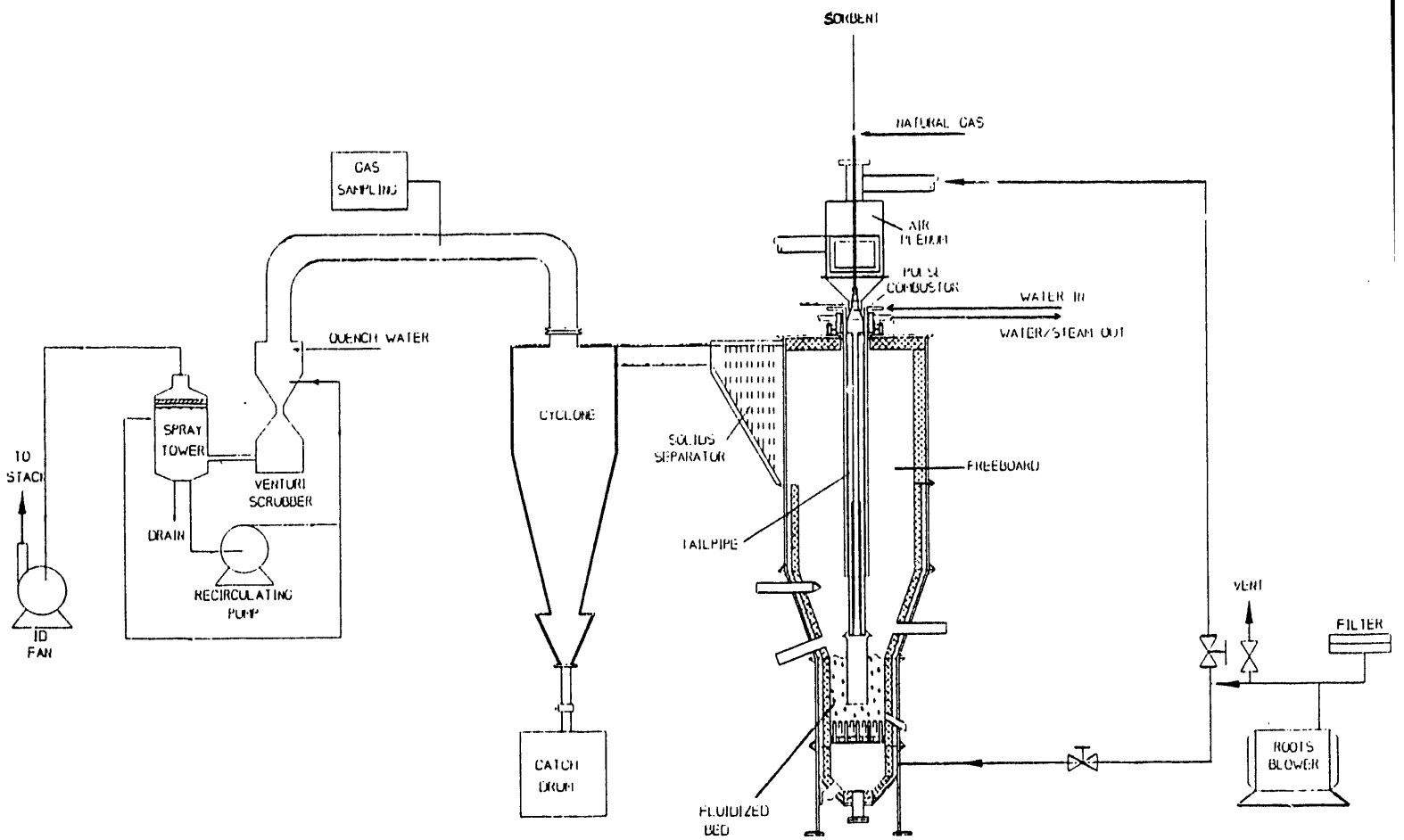

FIGURE 5: PAFBC FACILITY FOR CALCINATION AND CLASSIFICATION OF SORBENT

The pulse combustor needs some repair; before attempting this repair, it was decided to evaluate the suitability of the PAFBC system for sorbent calcination and classification by firing gas in the bed and freeboard area to check the temperature profile in the system and the ability to reach temperatures of 1500 - 1600°F.

The MTCI PAFBC system was tested (without pulse combustor) by firing gas in the bed windbox and freeboard area to check temperature profile along the system. Temperatures in excess of 1400°F were reached in the bed area. Therefore, repair of the pulse combustor was accomplished and the combustor was installed into the system. A limestone feeder with a feed rate controller and a feed line with eductor were installed. A test with 0.7 MMBtu/hr gas firing rate in the pulse combustor and an 0.8 MMBtu/hr in the bed windbox was performed with 40 lb/hr limestone feed rate into the pulse combustor. A temperature in the bed area of 1450°F was achieved but limitations in cooling water supply did not allow further increase in firing rate and temperature. A new water line, separate from the pulse combustor water jacket line, was installed for cooling the bed distributor plate, solids separator and cyclone. Inspection of the cyclone catch pot after the test showed that the cyclone was plugged by limestone. The solids separator and the cyclone cooling water systems, therefore, were connected in series with the exit from the solids separator connected to the inlet of the cyclone to keep the temperature of the bottom of the cyclone above the dew point of flue gas. Also, two sloped drain pipes from the bottom of the cyclone were cut off and replaced by one vertical pipe to facilitate ease of solids flow into the catch pot.

2.2 AEROVALVE TEST (WEST VIRGINIA UNIVERSITY)

2.2.1 VORTEX AEROVALVE GEOMETRY

Figure 6 is a drawing of a typical vortex-type aerovalve, and Figures 7 through 9 are the sketches used to derive the geometry relations for the valve. The graphs shown in Figures 10 through 13 are the results of the QuickBasic computer program. Figure 10 is a plot of the area ratio A_r versus the diffuser throat width s_{th}/r_o, in this case for N = 8 throats. Figure 11 is the same graph for N = 12 throats. Notice that in both cases for $\theta = 15^\circ$ there is a maximum A_r of ~ 2.25 and 2.75, respectively. Figures 12 and 13 are plots of the area ratio versus the total nondimensional throat area.

2.2.2 VORTEX AEROVALVE DESIGN

To limit the valve design to reasonable vane passage area ratios and to achieve a significant increase in angular velocity of the reverse flow, the independent program parameters were modified. The following independent parameters control the geometry of the aerovalve.

- To bring the vortex cross-sectional area in line with that of the vane passages, one needs a large number of vanes, say N = 8 or 12, which is selected as an input parameter.

- The parameter θ controls the vane offset from the radial direction ($\theta = 0^\circ$ for a radial blade) and is usually in the range $5^\circ < \theta < 25^\circ$.

- To achieve a significant increase in angular momentum one must keep the vane curvature radius r_c/r_o within reasonable geometry limits, typically $0.5 < r_c < 1.0$.

The performance of the aerovalve is calculated for a specific geometry.

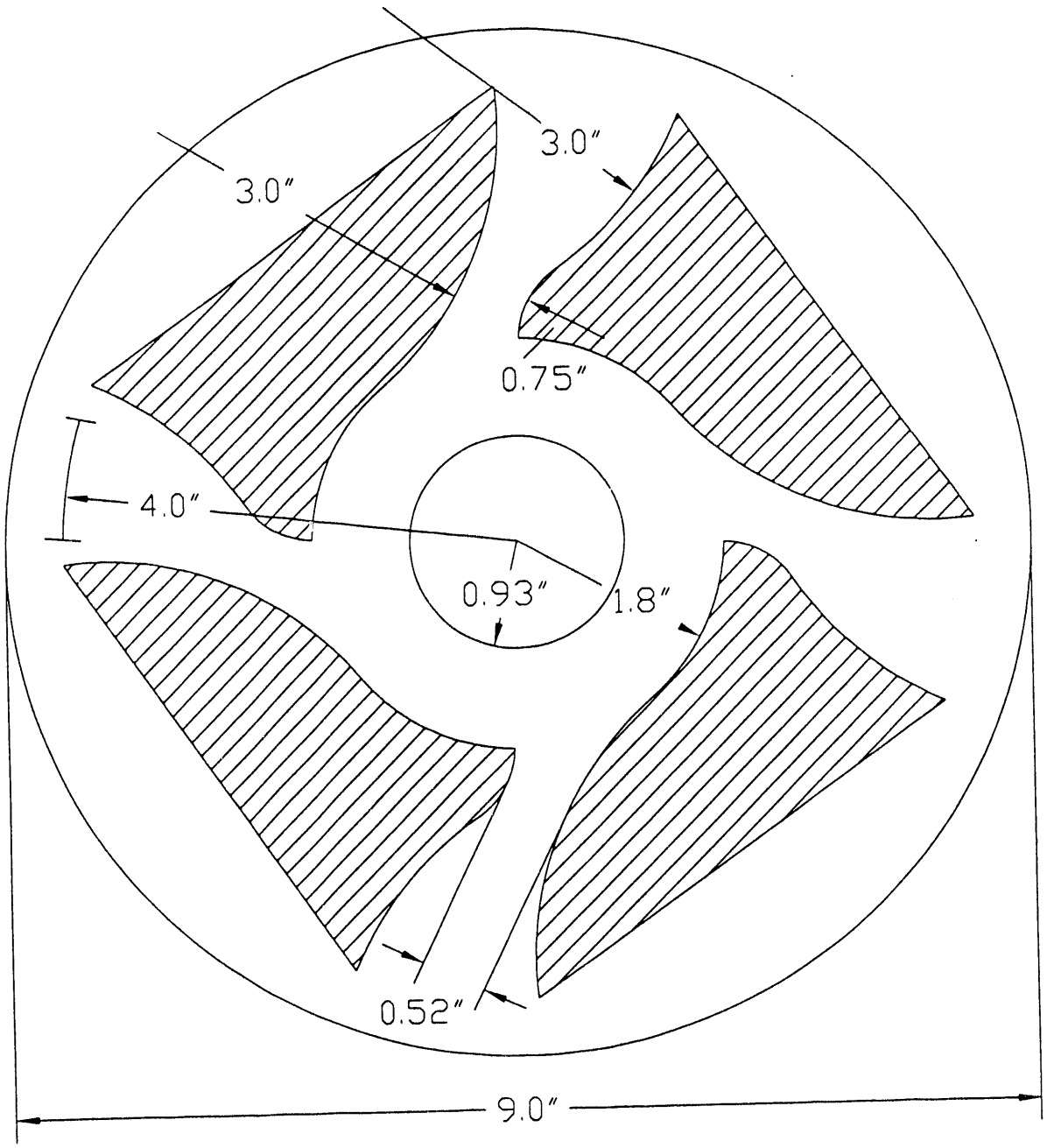

FIGURE 6: PROPOSED VORTEX AEROVALVE FOR VITIATED AIR PULSE COMBUSTOR

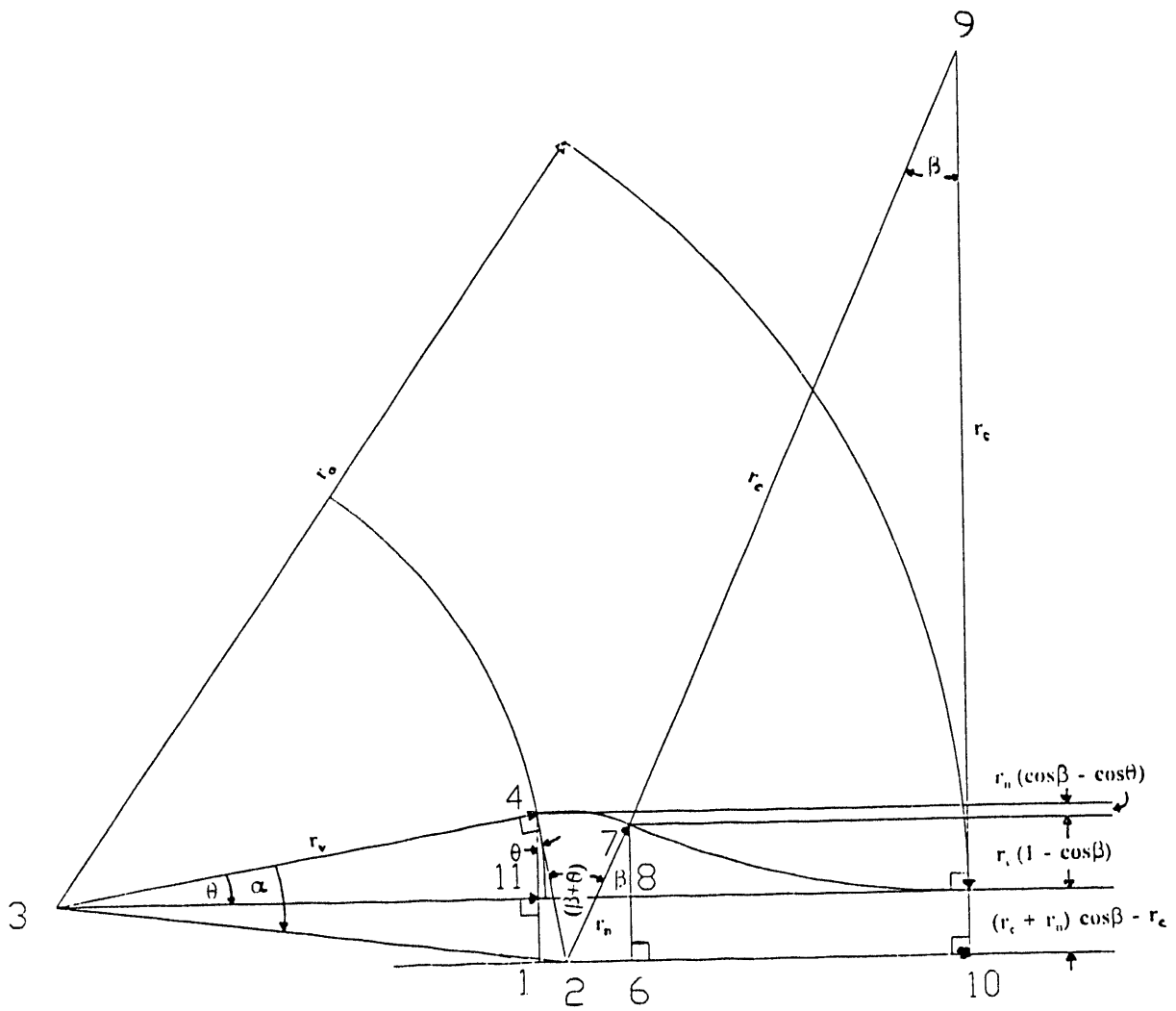

FIGURE 7: AEROVALVE 5 GEOMETRY

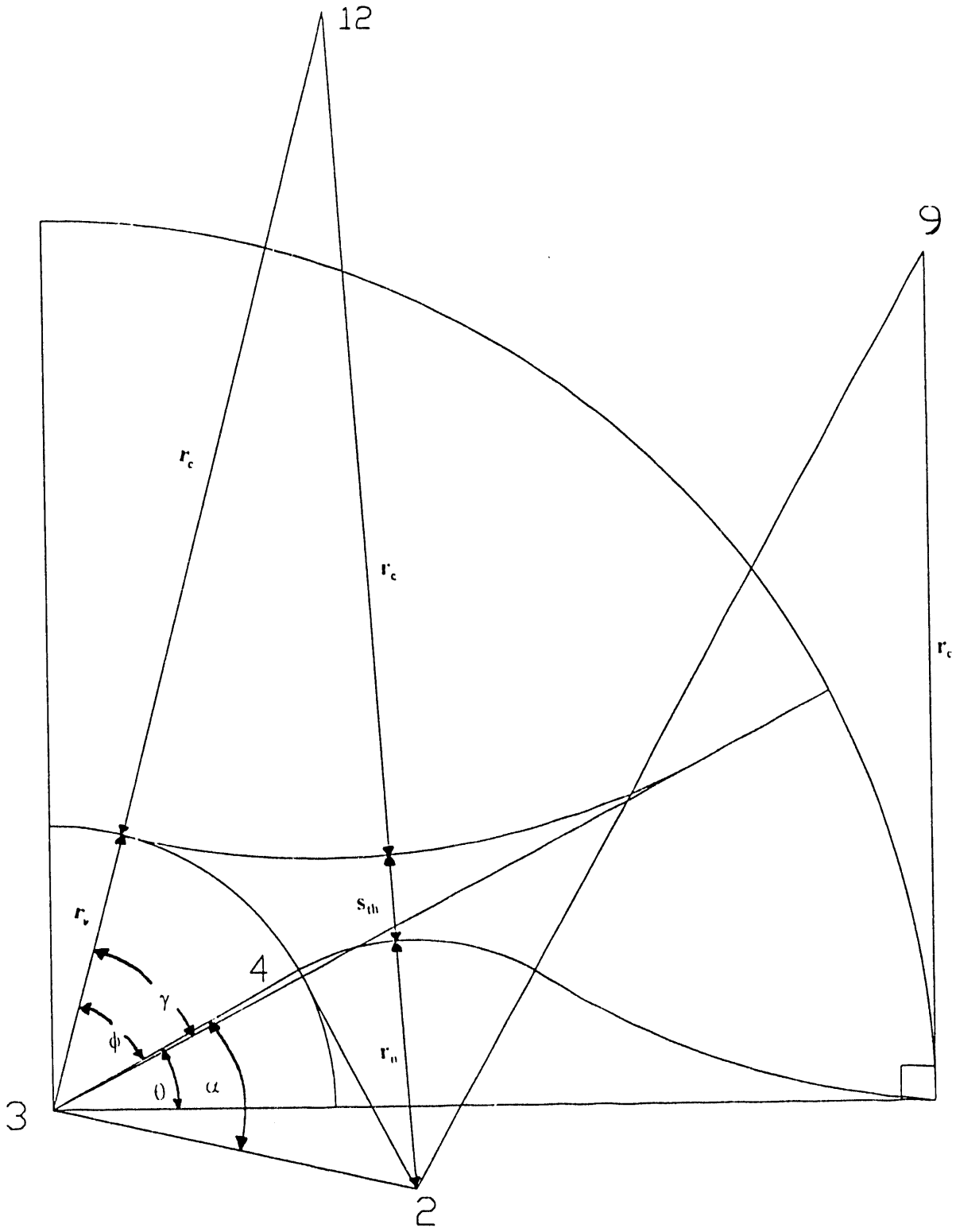

FIGURE 8: AEROVALVE 5 GEOMETRY USED IN THROAT WIDTH AND AREA RATIO DERIVATION

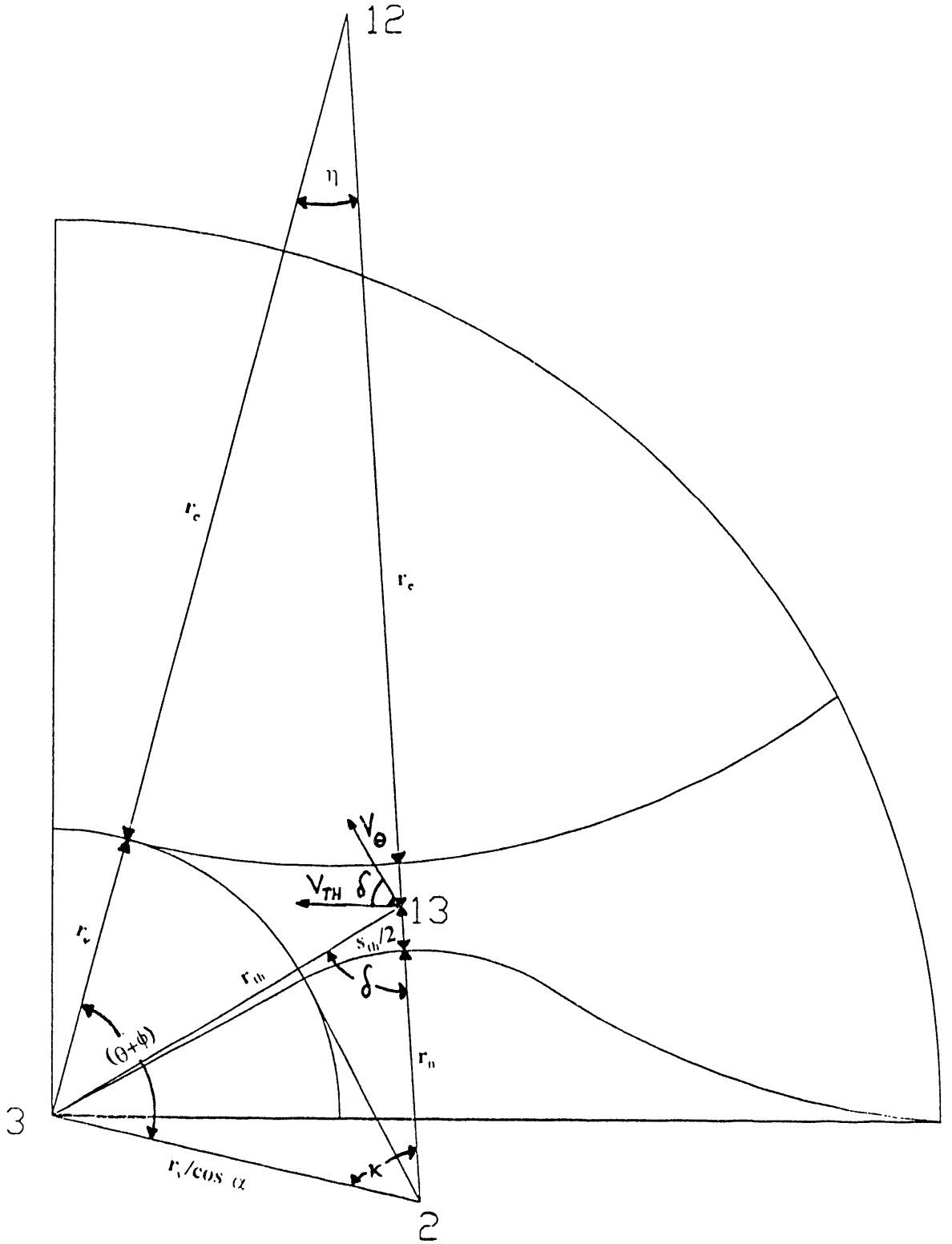

FIGURE 9: AEROVALVE 5 GEOMETRY USED IN THROAT RADIUS DERIVATION

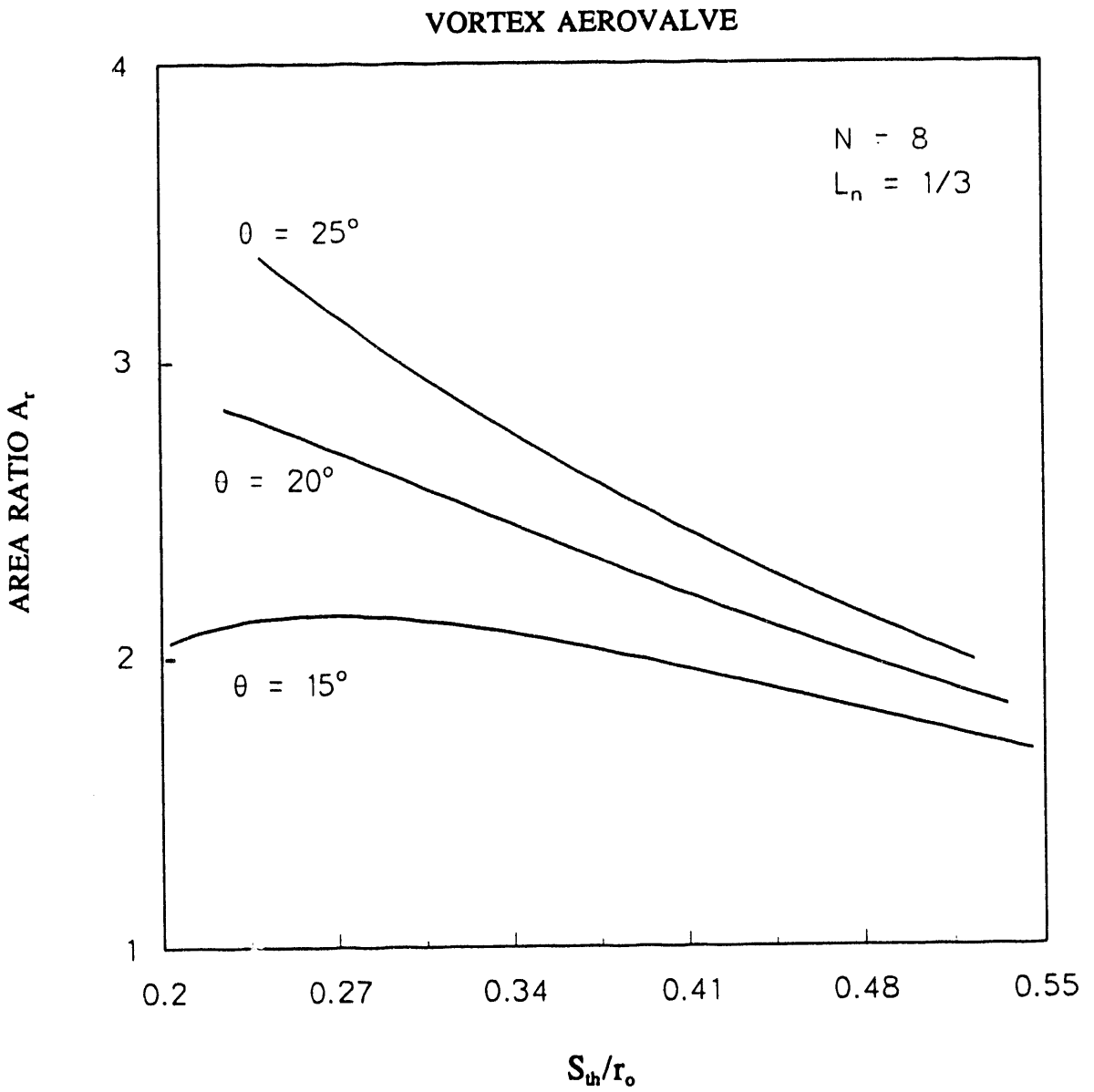

FIGURE 10: PLOT OF AREA RATIO vs. DIFFUSER THROAT WIDTH FOR N = 8

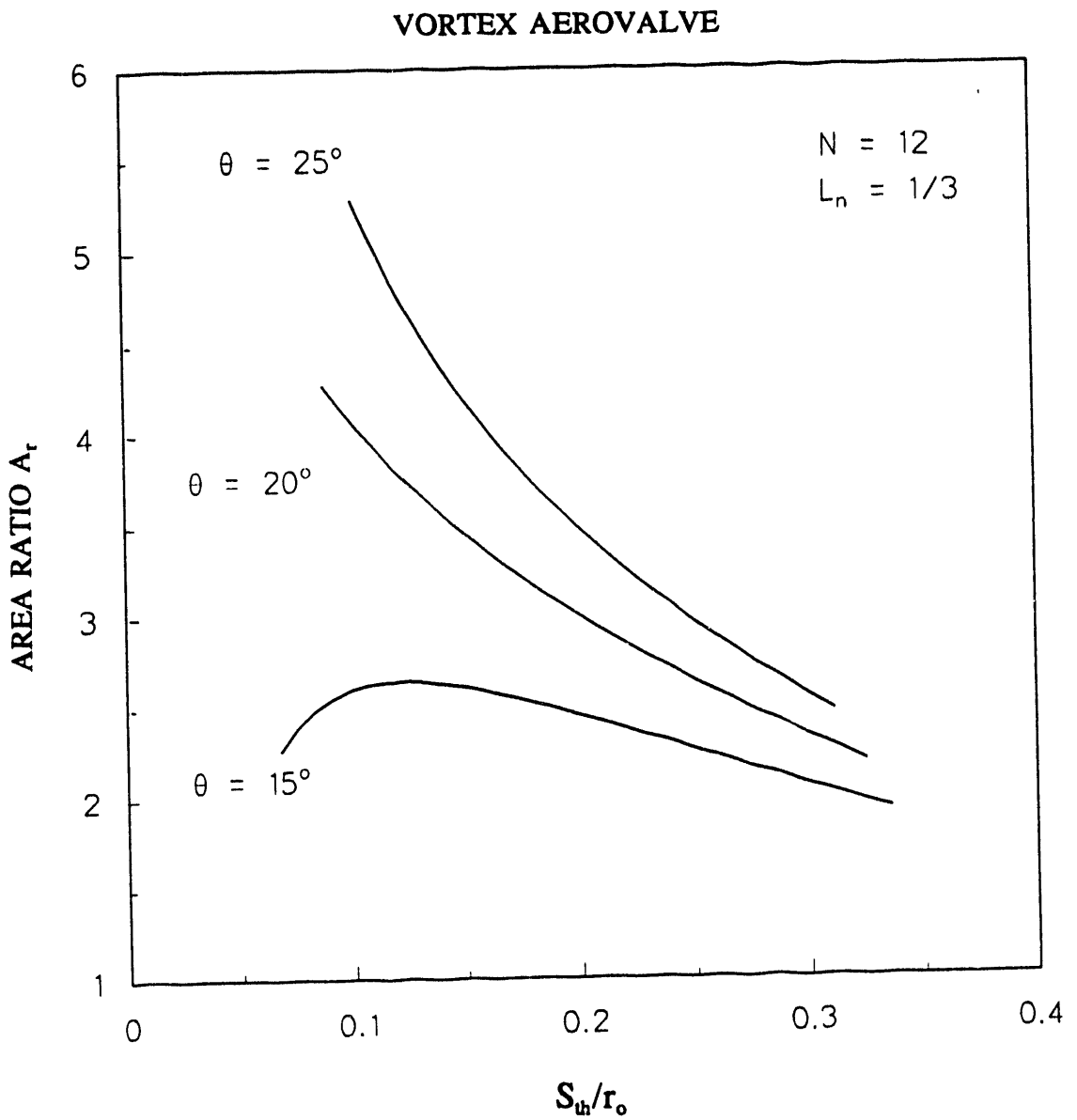

FIGURE 11: PLOT OF AREA RATIO vs. DIFFUSER THROAT WIDTH FOR N = 12

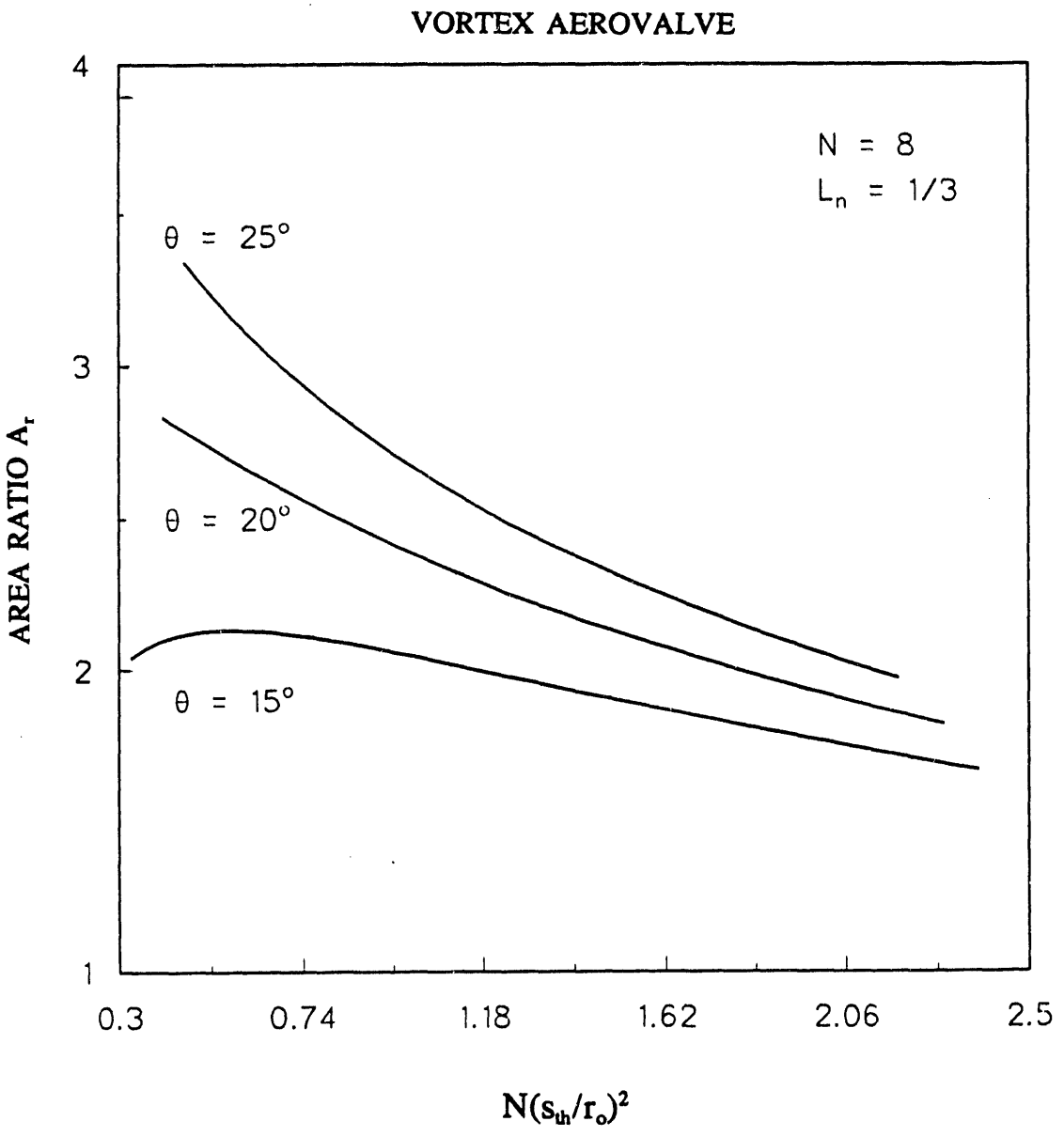

FIGURE 12: PLOT OF AREA RATIO vs. NON-DIMENSIONAL THROAT AREA FOR N = 8

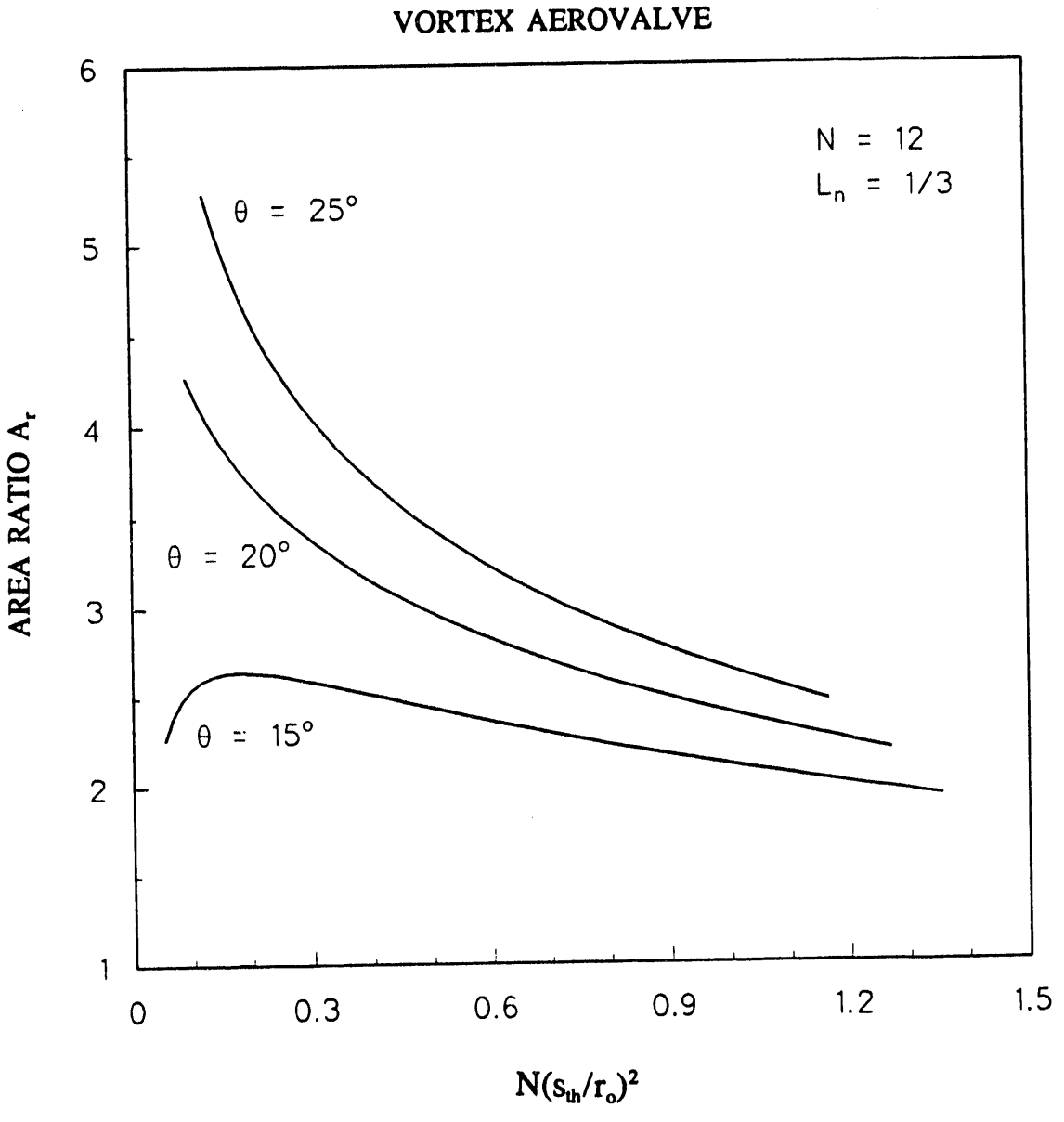

FIGURE 13: PLOT OF AREA RATIO vs. NON-DIMENSIONAL THROAT AREA FOR N = 12

Several modifications to the theory presented in the June report are described next. Recall that the diodicity of the aerovalve was defined as the ratio of forward to reverse mass flow rates, so

$$\Delta p_f = \Delta p_r \tag{2.1}$$

The expression for the forward flow pressure loss Δp_f is given by

$$\Delta p_f = \frac{1}{2} \rho V_{e_f}^2 \qquad \left(V_{e_f} = \frac{V_{th_f}}{A_r} \right) \tag{2.2}$$

where $V_{th\ f}$ is the forward flow throat velocity and A_r is the vane area ratio. The mass flow rate in forward flow is given by

$$\dot{m}_f = N s_{th}^2 \rho V_{th_f} \tag{2.3}$$

Recall that the vane area ratio in Equation 2.2 was given by the expression

$$A_r = \frac{\phi + \theta - \gamma}{s_{th}} \tag{2.4}$$

The forward flow pressure loss becomes

$$\frac{\Delta p_f}{\frac{1}{2}\rho} = \left(\frac{V_{th_f}}{A_r}\right)^2 \tag{2.5}$$

The reverse flow pressure loss Δp_r is given by

$$\Delta p_r = \frac{1}{2}\rho V_{e_r}^2 \tag{2.6}$$

The reverse flow exit velocity $V_{e\,r}$ is composed of two terms: $V_{r\,i}$ and $V_{\theta\,i}$. The relationship is

$$V_{e_r}^2 = V_{r_i}^2 + K_r V_{\theta_i}^2 \tag{2.7}$$

The term K_r is set equal to 1. The effect of K_r will be investigated later; it includes the viscous losses in the valve. The radial component $V_{r\,i}$ was determined using two different methods:

- Case 1: The pressure on the cylindrical surface of revolution with radius r_i which extends from the inlet to the back face of the valve was assumed to be the ambient pressure ($p = p_{AMB}$),
- Case 2: $V_{r\,i}$ was replaced by a uniform axial component V_z such that $V_z \pi r_i^2 = N V_{th} s_{th}^2$, where V_z is uniform over the opening.

For case 1, V_{r_i} was determined from the mass flow rate

$$V_{r_i} = \left(\frac{\dot{m}_r}{\rho 2\pi r_i s_{th}}\right)^2 \quad where \quad \dot{m}_r = V_{th} N s_{th}^2 \rho \ , \tag{2.8}$$

For case 2, V_z was determined from

$$V_z \pi r_i^2 = N V_{th_r} s_{th}^2 \tag{2.9}$$

Using the conservation of angular momentum the expression for V_{θ_i} was found to be

$$\begin{gathered} V_{\theta_{r,th}} r_{th} = V_{\theta_i} r_i \quad where \quad V_{\theta_{r,th}} = V_{th_r} \cos\delta \\ V_{\theta_i} = \frac{r_{th}}{r_i} V_{th_r} \cos\delta \end{gathered} \tag{2.10}$$

Substituting the expressions for V_{r_i} and V_{θ_i} from Equs. 2.8 and 2.10 and the expression for the reverse flow mass flow rate from Equation 2.8 into Equation 2.7, the expression for V_{e_r} for case 1 was obtained:

$$V_{e_r}^2 = \left(\frac{V_{th_r} N s_{th} \rho}{\rho 2\pi r_i s_{th}}\right) + K_r \left(\frac{r_{th}}{r_i} V_{th_r} \cos\delta\right)^2 \tag{2.11}$$

Similarly, for case 2, the substitution of the expression for V_z (replacing V_{r_i}) from Equation 2.9 into Equation 2.7 yielded

$$V_{\theta_r}^2 = \left(\frac{V_{th_r} N s_{th}^2}{\pi r_l^2}\right)^2 + K_r\left(\frac{r_{th}}{r_l} V_{th_r} \cos\delta\right)^2 \qquad (2.12)$$

A design condition for the aerovalve was that

$$2\pi r_l s_{th} = K N s_{th}^2 \qquad (2.13)$$

where K is the area ratio of the entire aerovalve. The diodicity D_v, assuming incompressible flow, was obtained by equating the forward and reverse flow pressure loss expressions and solving for the ratio of forward to reverse flow throat velocities. After some algebraic manipulation, two slightly different expressions were obtained:

Case 1:

$$D_v = A_r K_{v_1}, \quad \text{where} \quad K_{v_1} = \sqrt{\left[\left(\frac{N s_{th}}{2\pi r_l}\right)^2 + K_r\left(\frac{r_{th}}{r_l}\cos\delta\right)^2\right]} \qquad (2.14)$$

Case 2:

$$D_v = A_r K_{v_2}, \quad \text{where} \quad K_{v_2} = \sqrt{\left[\left(\frac{N s_{th}^2}{\pi r_l}\right)^2 + K_r\left(\frac{r_{th}}{r_l}\cos\delta\right)^2\right]} \qquad (2.15)$$

These modifications were added to the existing program and the results are shown in Figures 14 to 19. Figures 2 to 4 were used in the derivation of the geometry of the valve. Figures 14 and 15 are plots of the vane area ratio A_r versus the vane inlet radius r_v/r_o for N = 8 and N = 12 throats, respectively. From these two figures it is seen that for decreasing r_c/r_o and an area ratio restricted to the range of $1.5 < A_r < 2.5$, r_v/r_o increases. Figures 16 and 17 show the graphs of multiplier K_v versus r_v/r_o for N = 8 and N = 12 throats. It is seen here that for increasing r_v/r_o and decreasing r_v/r_o the values of K_v decrease. The major difference between 8 and 12 throats is shown by the fact that the highest value of K_v for 8 throats is ~ 0.95, while for 12 throats and the same value of r_c/r_o the highest value is ~5.5, almost 5.5 times greater. Figures 18 and 19 show the diodicity D_v versus r_v/r_o and, of course, the diodicity is seen to be higher for 12 throats than for 8.

Figure 20 is a drawing of the valve with the geometry indicated on Figures 15, 17 and 19 by a "•" on the curve.

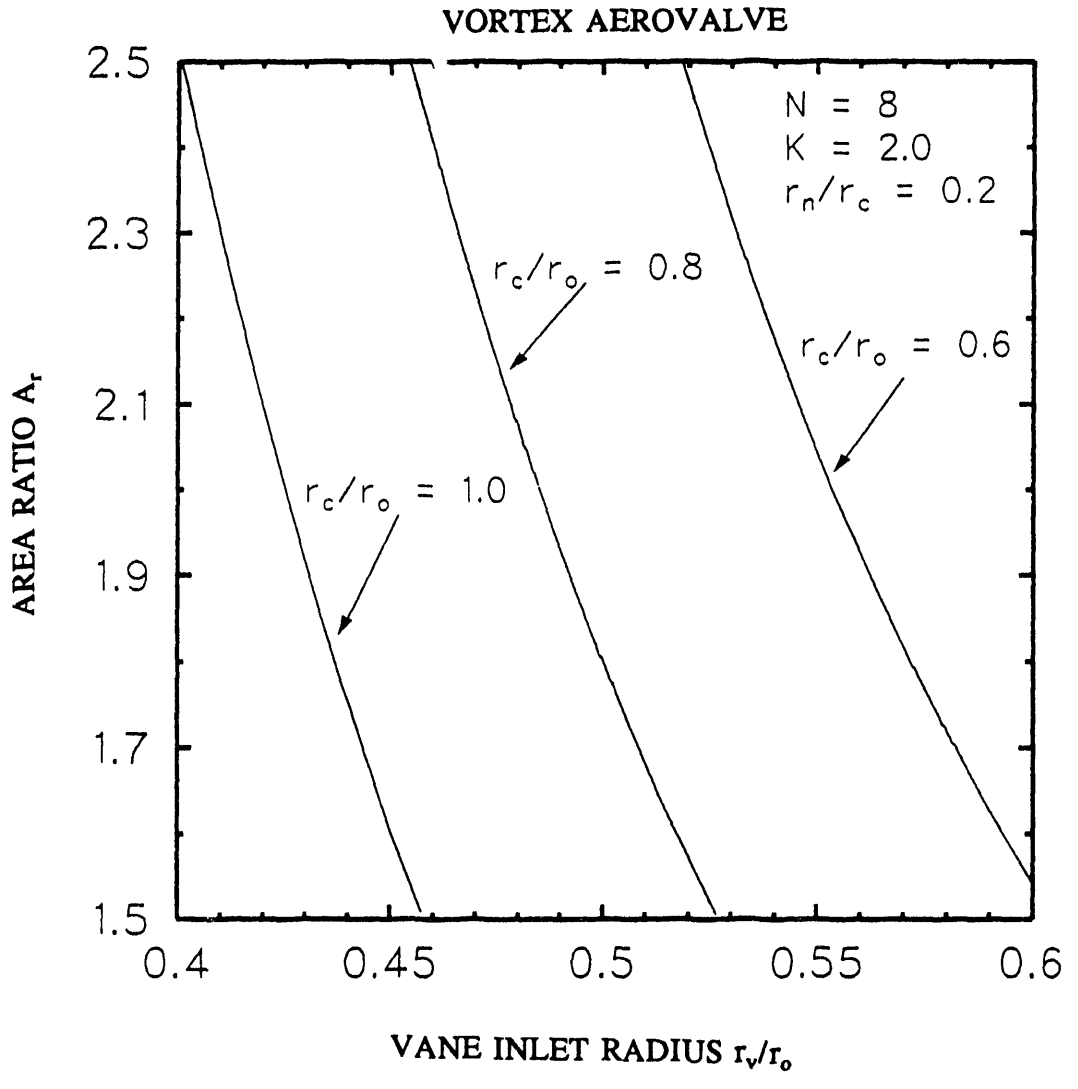

FIGURE 14: PLOT OF AREA RATIO vs. VANE INLET RADIUS FOR N = 8 THROATS

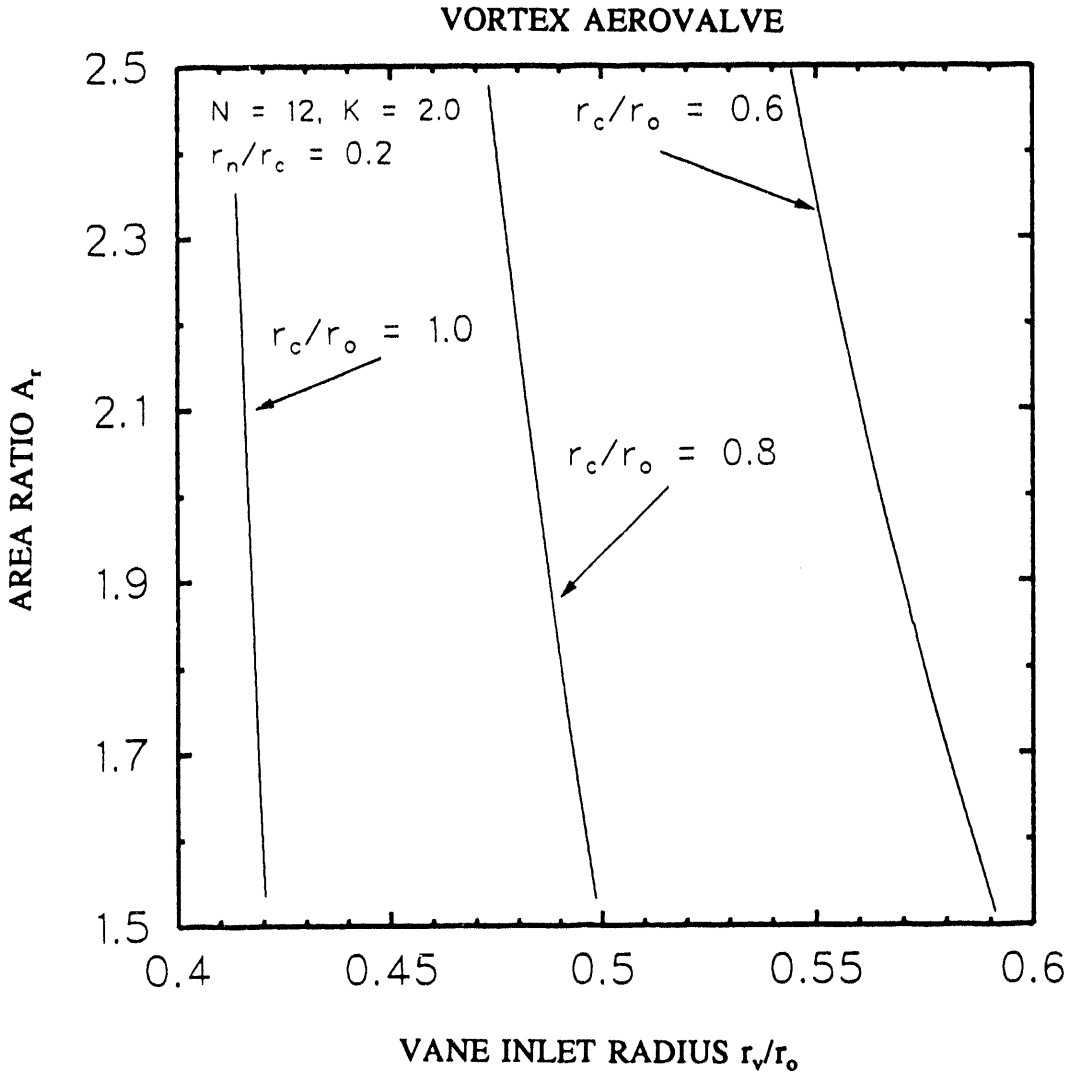

FIGURE 15: PLOT OF AREA RATIO vs. VANE INLET RADIUS FOR N = 12 THROATS

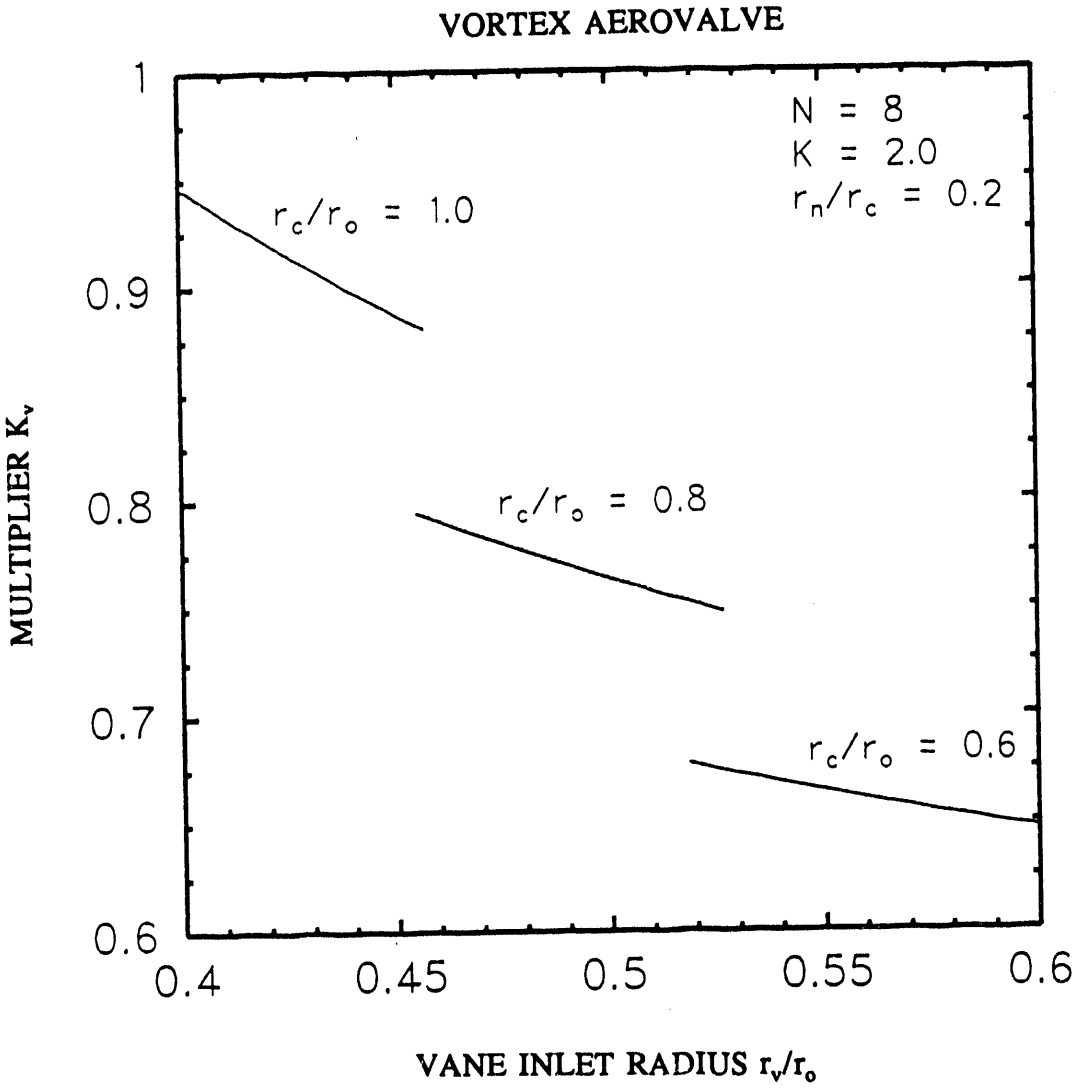

FIGURE 16: PLOT OF MULTIPLIER K_v vs. VANE INLET RADIUS FOR N = 8 THROATS

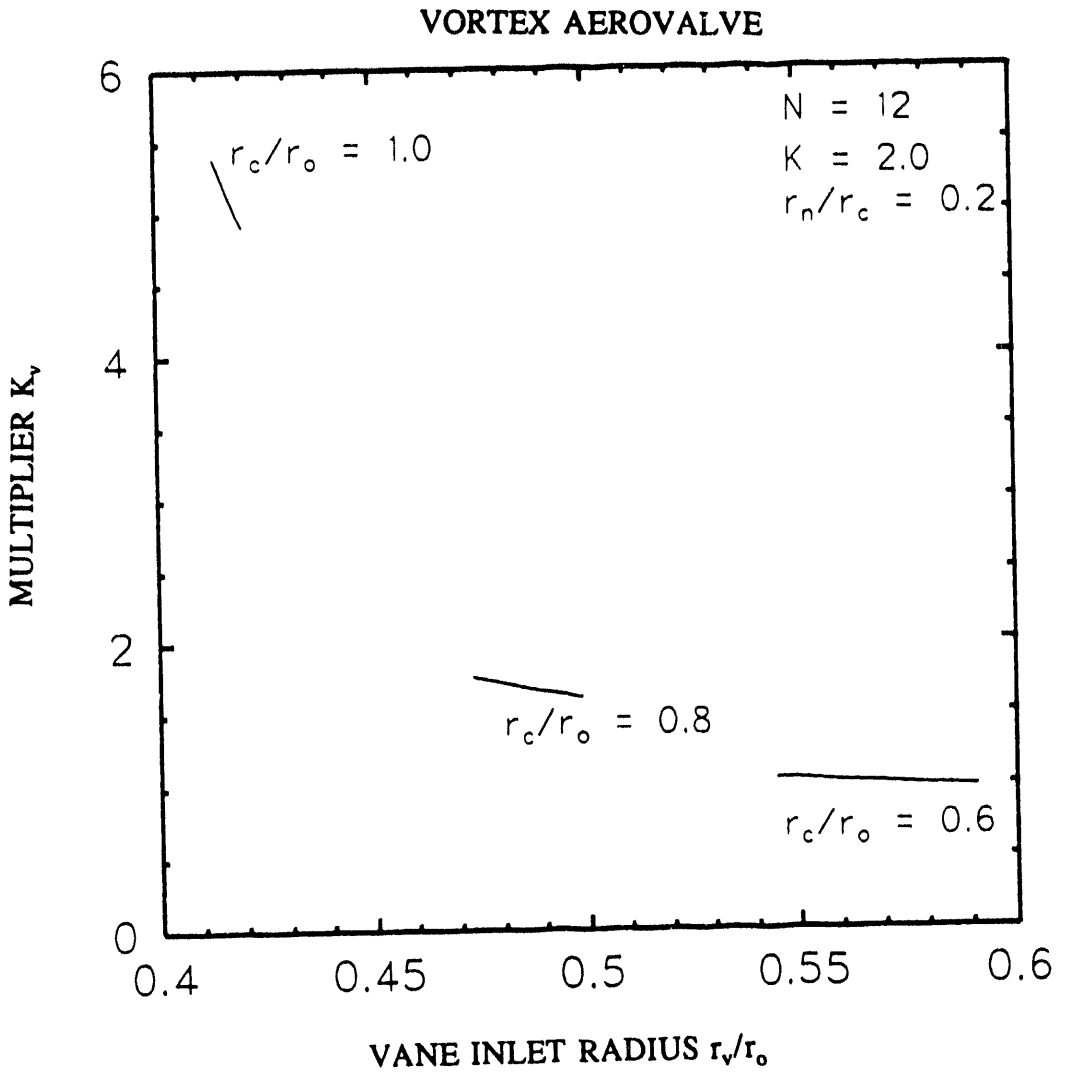

FIGURE 17: PLOT OF MULTIPLIER K_v vs. VANE INLET RADIUS FOR N = 12 THROATS

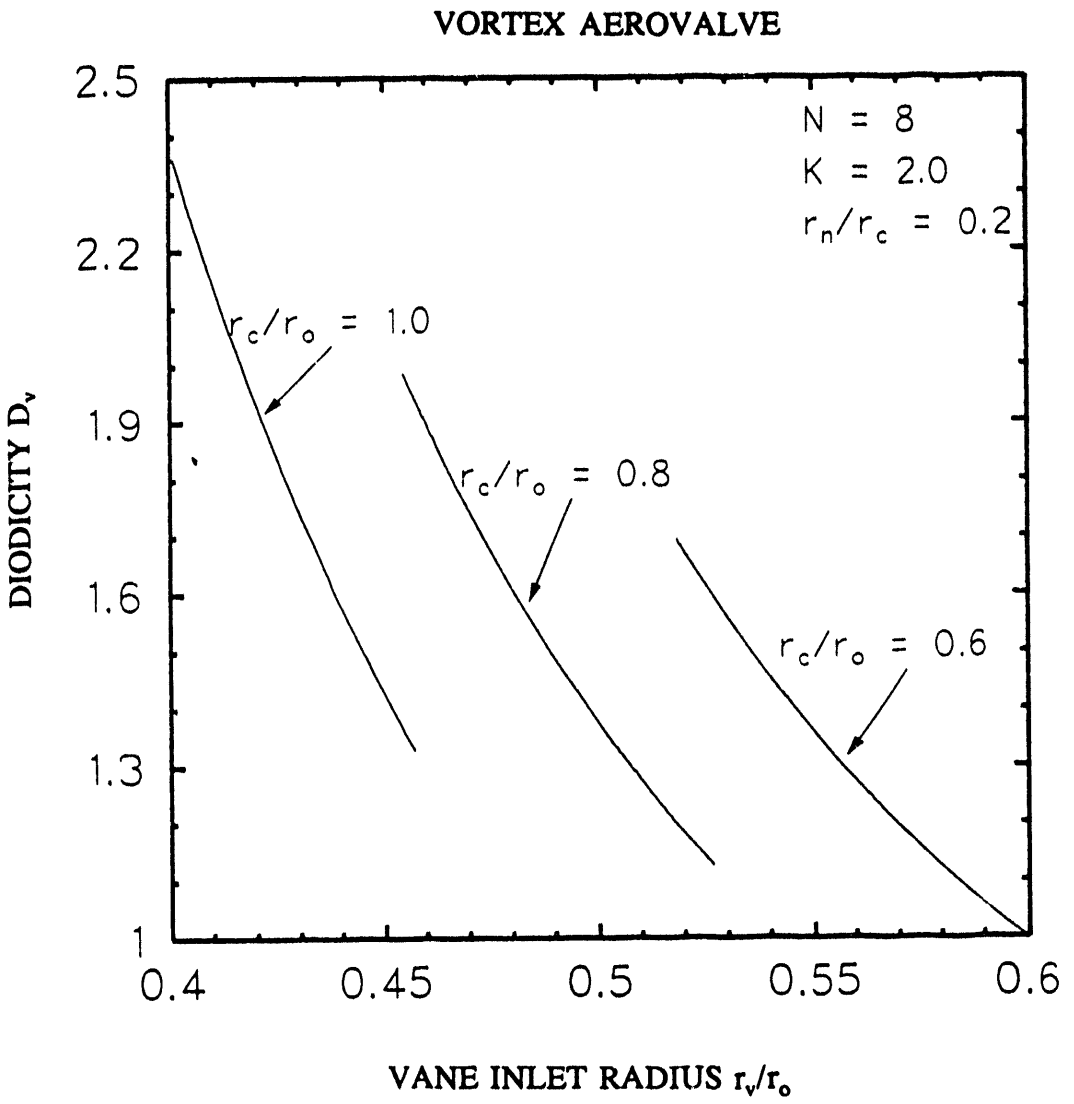

FIGURE 18: PLOT OF THEORETICAL DIODICITY D_v vs. VANE INLET RADIUS FOR N = 8 THROATS

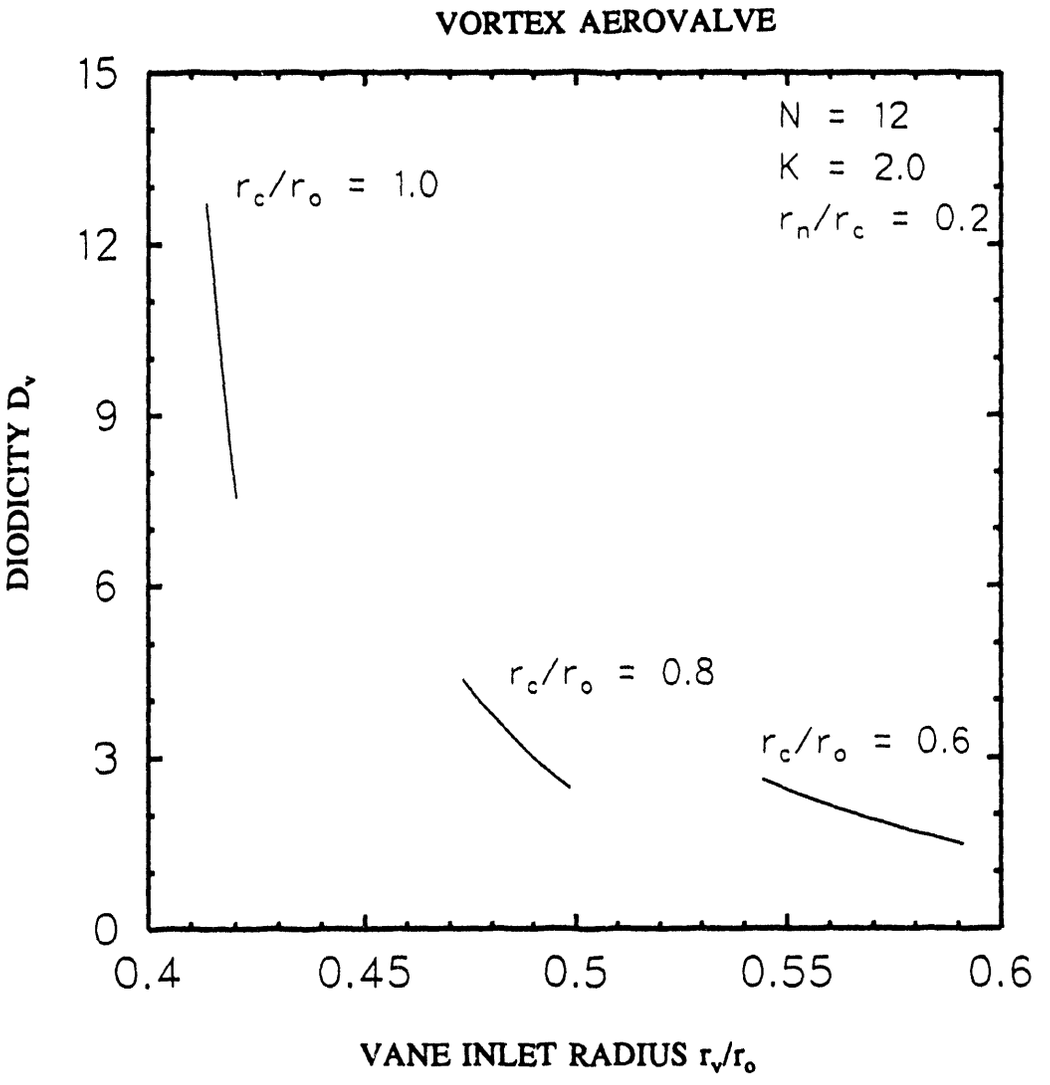

FIGURE 19: PLOT OF THEORETICAL DIODICITY D_v vs. VANE INLET RADIUS FOR N = 12 THROATS

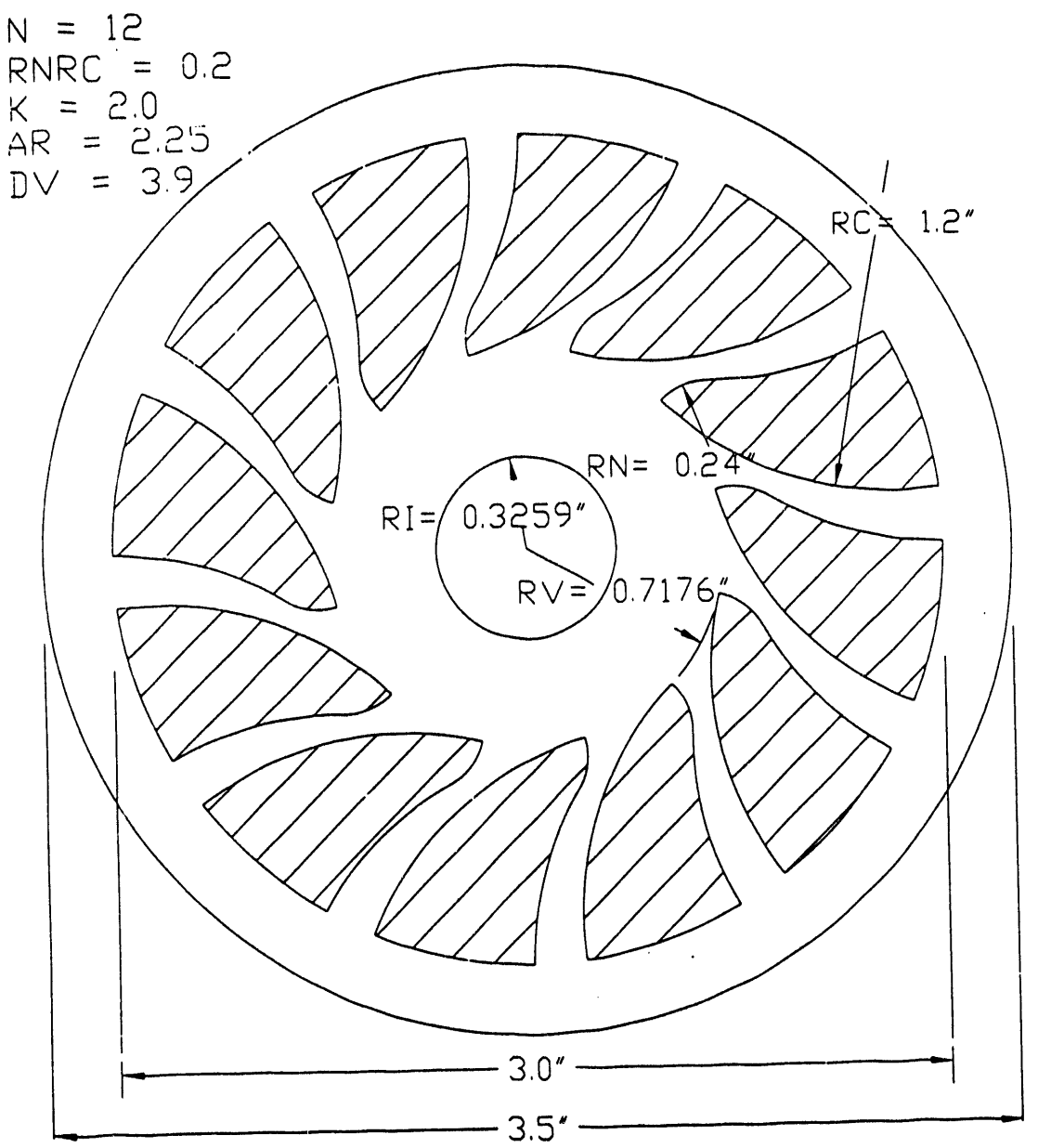

FIGURE 20: PROPOSED VORTEX AEROVALVE FOR VITIATED AIR PULSE COMBUSTOR

2.3 FUNDAMENTAL SORBENT STUDIES (PENN STATE UNIVERSITY)

The objective of the Penn State Task 1 is to conduct a fundamental study of the physical and chemical changes that calcium-based sorbents undergo when subjected to high heating rates for short residence times to determine if a flash calcination phenomenon occurs producing a highly reactive calcine. Subsequent sulfation of the calcine will also be studied.

In Task 2, Penn State will conduct a fundamental study of bimodal acoustic agglomeration in two stages. In the first stage, an entrained-flow reactor (EFR) will be used to optimize the frequency and sound pressure level for a range of fly ash and sorbent mass loadings, particle sizes and reactor temperatures. The focus of the experiments in the second stage of the agglomeration investigation will be to identify experimentally the mechanisms that control the bimodal agglomeration and cohesion of fly ash and sorbent particles under the influence of a high-intensity acoustic field.

In Task 3, Penn State will combine the results from the two fundamental studies above into one model to predict sulfur capture and bimodal acoustic agglomeration under pulse combustion conditions. As experimental data become available from Tasks 1 and 2, progress on Task 3 will be reported.

2.3.1 FUNDAMENTAL STUDY OF SORBENT BEHAVIOR

Preliminary pulse combustion tests by MTCI using a dolomite for sulfur capture showed that four times (i.e., 400 ppmw) the acceptable level of fines were present in the exit gas stream. The level of sulfur capture was considered acceptable (> 90%). MTCI concluded that the fines were generated by the fragmentation of the dolomite during calcination. Penn State recommended that a test using a limestone be conducted based on the known fragmenting behavior of limestones versus dolomites upon calcination. Tests conducted at Penn State have shown that dolomites are more susceptible than limestones to breakage when subjected to high heating rates. Dolomites contain calcium and magnesium carbonates. The mechanism of the fragmentation involves the decomposition of the calcium magnesium carbonate ($CaMg(CO_3)_2$) into $CaCO_3$ and $MgCO_3$. The magnesium carbonate rapidly decomposes into magnesia releasing carbon dioxide. The calcite

subsequently decomposes to lime and carbon dioxide. The high CO_2 pressure within the particles is sufficient to overcome their mechanical strength. The decomposition of the magnesium carbonate is much more rapid than that of calcium carbonate. This two-stage evolution of carbon dioxide contributes to the extensive fragmentation of dolomite particles.

Penn State suggested using the Linden Hall limestone in a combustion test at MTCI. The Linden Hall limestone has a calcium carbonate content of approximately 99.5 percent.

MTCI tested the Linden Hall limestone in the pulse combustor. The limestone produced approximately one-half of the concentration of fines (i.e., 200 ppmw) produced during tests using dolomite as a sulfur capture agent. This was in direct agreement with the experimental work using laser heating techniques conducted at Penn State. The sulfur removal by the limestone was greater than 90 percent.

Concern for the concentration of fine particles in the gas stream prompted MTCI to investigate the use of lime as a sulfur capture agent. A sample of lime that will be tested in the MTCI pulse combustor was received from MTCI. Particle size and chemical analysis of the lime will be conducted.

The chemical analysis of the lime provided by MTCI is given in Table 1.

It was necessary to determine the particle size distribution of the lime by using sonic sieving in combination with a Malvern Particle Size Analyzer since the particles were too coarse to be sized by Malvern alone. Particle size data determined by sonic sieving is given in Table 2. A cumulative frequency curve is given in Figure 21.

TABLE 1:
LIME COMPOSITION

OXIDE	WEIGHT %
SiO_2	2.10
Al_2O_3	0.90
TiO_2	0.04
Fe_2O_3	0.28
MnO	0.01
CaO	89.00
MgO	1.25
Na_2O	<0.05
K_2O	0.16
P_2O_5	<0.02
SO_3	<0.02
BaO	<0.02
SrO	<0.02
LOI	7.03
TOTAL	100.80

TABLE 2:
PARTICLE SIZE DISTRIBUTION OF LIME DETERMINED BY SONIC SIEVING

SIZE (μm)	CUMULATIVE WEIGHT %
45	14.63
75	23.89
106	29.49
150	33.72
212	38.24
355	45.77
500	52.80
710	60.26
1180	76.61
1700	90.17
2800	100.00

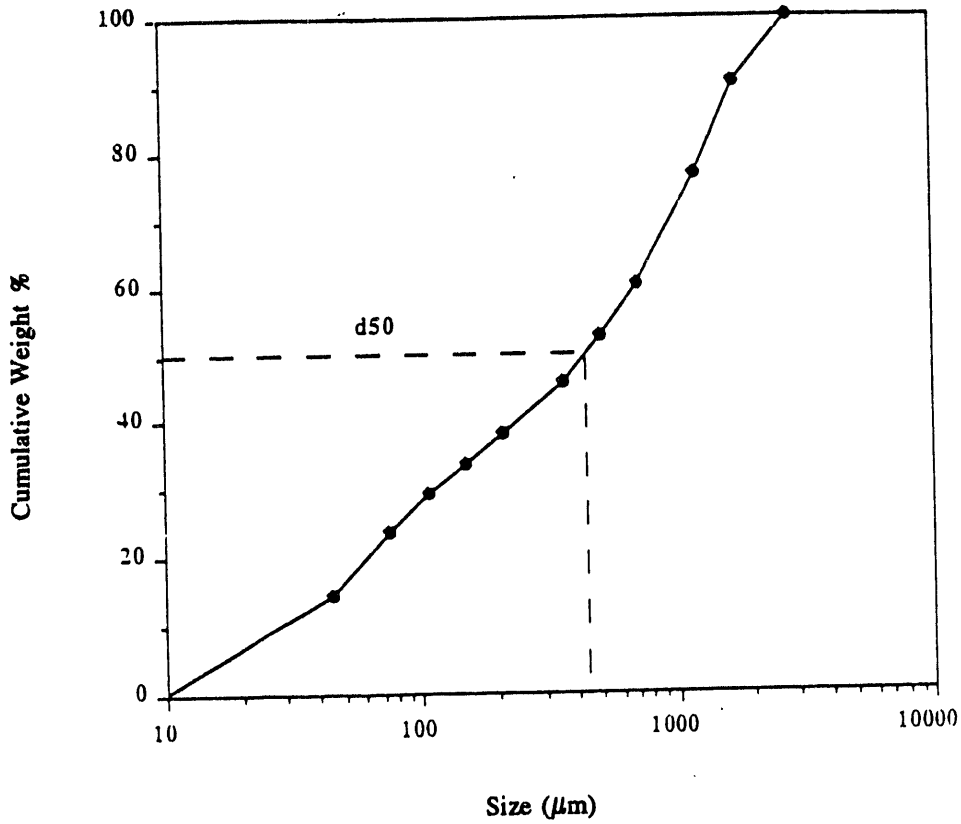

FIGURE 21: PARTICLE SIZE DISTRIBUTION OF LIME (SONIC SIEVE)

The material is quite coarse. The top size of the material is between 1,700 and 2,800 μm. The largest particle size that can be measured by the Malvern at Penn State is 564 μm. A d_{50} of 442 μm can be interpolated from the curve in Figure 1. This material was chosen by MTCI to be tested in their pulse combustor. The decision to test the lime was based on MTCI's concern with the production of fines during calcination of limestone and dolomite. The intent of MTCI is to reduce the concentration of fines produced in the gas stream because of the coarse particle size distribution of the material.

The material that passed through the 45 μm screen was collected and sized by the Malvern. The particle size distribution is given in Table 3. The cumulative weight percent curve is shown in Figure 22.

TABLE 3:

PARTICLE SIZE DISTRIBUTION OF SIEVE FINES (<45 μM) OF LIME SAMPLE AS DETERMINED BY THE MALVERN

Size (μm)	Cumulative Weight %	Size (μm)	Cumulative Weight %	Size (μm)	Cumulative Weight %	Size (μm)	Cumulative Weight %
163	100.0	47.3	82.9	12.8	19.7	3.46	3.2
151	99.9	40.9	73.1	11.1	17.7	3.21	2.5
131	99.9	35.4	62.3	9.56	15.8	2.99	1.9
113	99.7	30.6	52.2	8.27	13.7	2.78	1.4
97.8	99.6	26.4	44.3	7.15	11.6	2.59	1.1
84.5	99.3	22.9	38.5	6.18	9.7	2.40	0.8
73.1	98.3	19.8	32.9	5.35	7.9	2.24	0.7
63.2	95.6	17.1	27.0	4.62	6.2	2.08	0.5
54.7	90.7	14.8	22.6	4.00	4.7	1.93	0.4

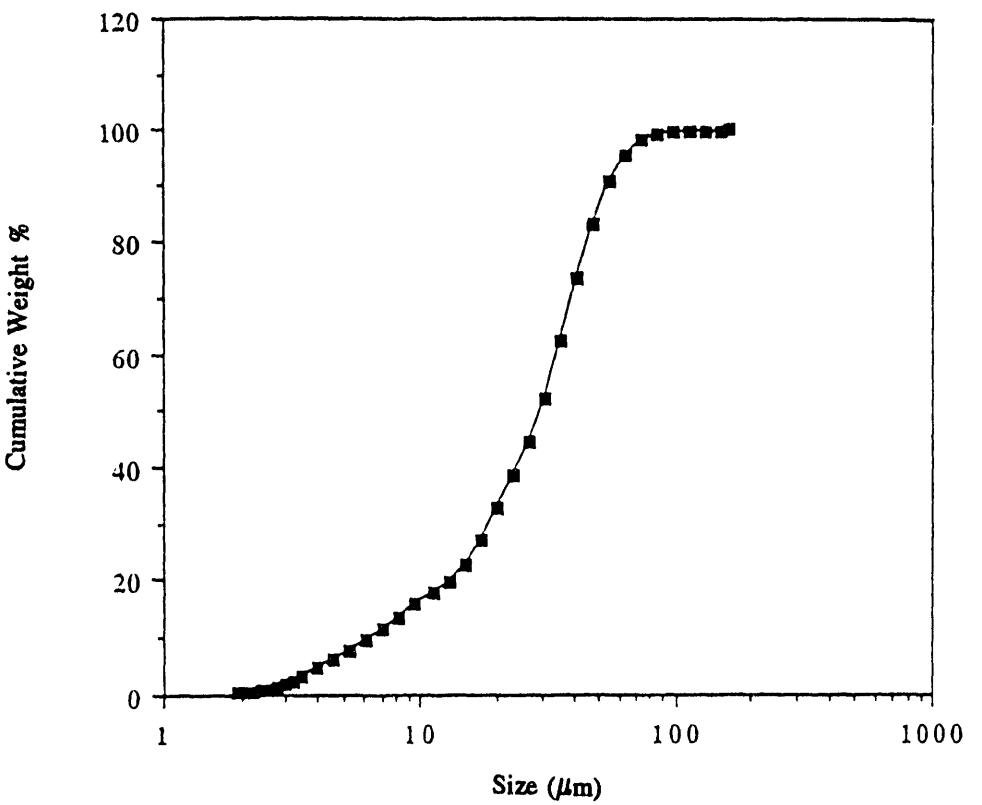

FIGURE 22: PARTICLE SIZE DISTRIBUTION OF SIEVE FINES (>45 μM) DETERMINED BY THE MALVERN

The d_{50} of the sieve fines is 29.5. Some particles measured by the Malvern are greater than 45 μm in diameter even though the material passed a 45 μm screen. This is due to differences in the manner in which sonic sieving and the Malvern size material.

Calcination of Limestone

MTCI is currently modifying the pulse combustor system to accommodate the calcination portion of the process. Their modifications are based on the results of the test runs using dolomite, limestone, and lime as sulfur capture agents in the pulse combustor. MTCI has informed Penn State that they will calcine the three stones (i.e., Linden Hall, Bossardville, and Nittany) once they have reconfigured their system. MTCI anticipates that modifications will be completed by September. During this time, Penn State will proceed with the calcination of the Linden Hall, Bossardville, and Nittany stones in the entrained flow reactor (EFR). Results of the initial calcination tests are given in Table 4.

TABLE 4:
RESULTS OF CALCINATION TESTS PERFORMED IN THE ENTRAINED FLOW REACTOR

		Entrained Flow Reactor Conditions				
Material	Size (μm)	Temperature (°C)	Gas Flow Rate (scfh)	Gas Velocity (m/s)	Gas Residence Time (s)	Calcination (%)
Linden Hall	74-105	1042	50	0.857	0.945	63.1
Bossardville	74-105	1045	50	0.859	0.943	72.7
Nittany	74-105	1048	50	0.861	0.940	76.2

Samples were collected at the exit of the EFR and represent the maximum extent of calcination attained given the residence time within the reactor at the given temperature. A probe will be designed to allow samples to be extracted at different positions within the EFR to study the effect of temperature and resi-

dence time on calcination. The probe will also be used during the sulfation test runs.

Additional calcination tests will be conducted based on MTCI's recommendations regarding the EFR test conditions.

The EFR modifications were completed and the reconstructed EFR used for the calcination tests in Task 1. The PCSV-P Insitec probe has been received by Penn State. The probe is currently being recalibrated. Beam power has been restored to 100 percent. Agglomeration tests will be resumed once the recalibration procedure has been completed. The tests conducted with acoustics at room temperature will be repeated to verify reproducibility and that the probe is operating properly.

The three sorbents have been sized into the following fractions: 270 x 400, 200 x 270, and 140 x 200 mesh (i.e., 37-53 μm, 53-74 μm, and 74-105 μm, respectively). Each size fraction will be calcined in the EFR to determine the effect of size on the extent to which particles calcine under given time temperature conditions. Samples will be extracted at different locations within the EFR to determine the effect of residence time on the extent to which each sorbent calcines. A sample collection probe was constructed for this purpose. In addition, a suction pyrometer was constructed for temperature measurements at the different sampling locations.

Calcination tests were started in the entrained flow reactor. The gas temperature profile of the reactor was determined. Reactor temperature profiles were determined for preheat temperatures of 900, 1000, and 1100°C. Temperatures were measured at the injector tip and along the isothermal zone of the reactor using a suction pyrometer (R-type thermocouple) at a suction rate of 128.7 cfh. The reactor temperature profiles as a function of preheat temperature as shown in Figure 23. The relationship between gas temperature and reactor wall temperature was also determined and is shown in Figure 24. The measured temperatures are given in Table 5. Establishing the relationship between gas and reactor temperature is necessary in order to determine the temperature history of calcine

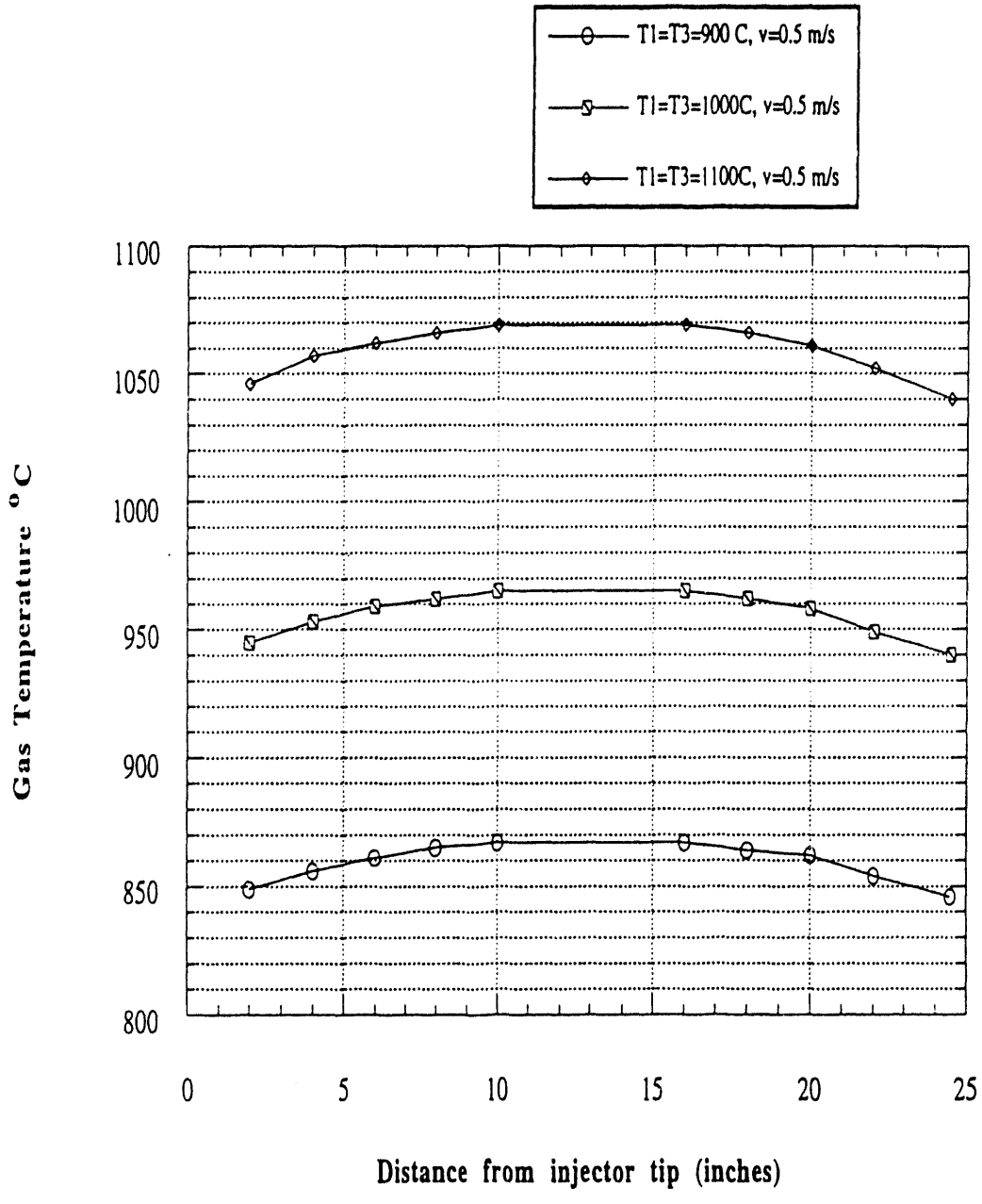

FIGURE 23: GAS TEMPERATURE PROFILE FOR VARIOUS PREHEAT TEMPERATURES

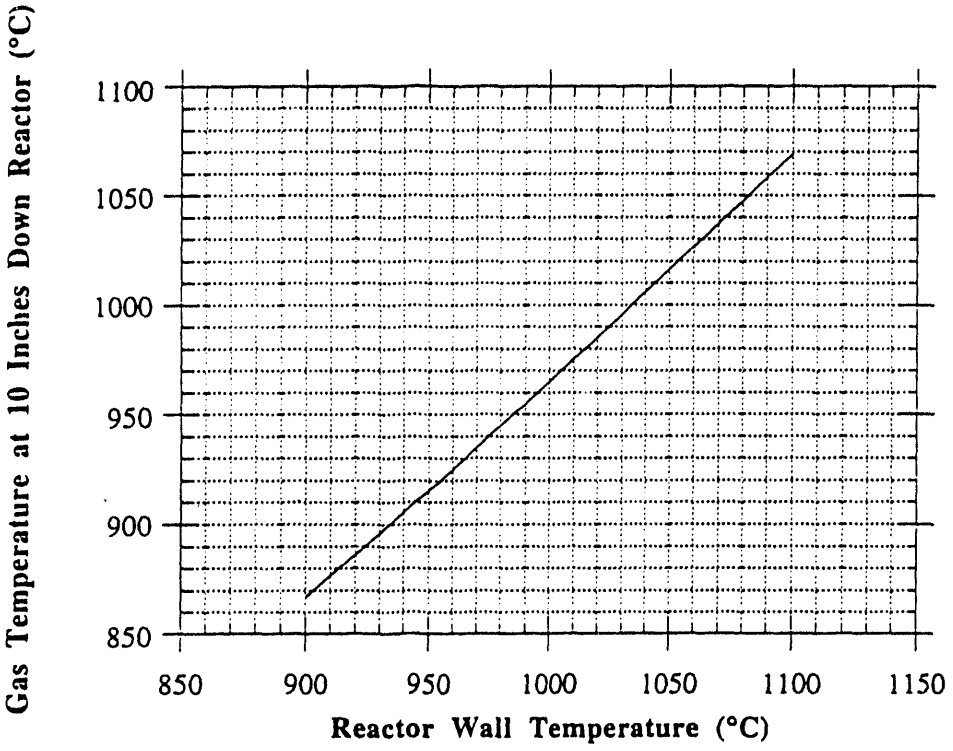

FIGURE 24: RELATIONSHIP BETWEEN GAS TEMPERATURES AND REACTOR WALL TEMPERATURE

TABLE 5:
TEMPERATURE DATA

	TEMPERATURE (°C)		
PREHEATER TEMPERATURE	900	1000	1100
INJECTOR TEMPERATURE	854	942	1021
REACTOR TEMPERATURE	900	1000	1100

particles within the reactor. Specific temperatures measured are given in Table 5. Gas velocities were calculated as a function of temperature and gas flow rates. A summary of the data is given in Table 6.

TABLE 6:
GAS FLOW RATES AND VELOCITIES AS A FUNCTION OF GAS TEMPERATURE

GAS TEMPERATURE (°C)	1000	1100
TOTAL GAS FLOW RATE ALONG THE REACTOR (CFH)	128.7	128.7
TOTAL GAS FLOW RATE AT STP (SCFH)	30.1	28.15
GAS FLOW RATE FOR SORBENT FEEDING (SCFH)	1.5	1.5
SECONDARY GAS FLOW RATE AT STP (SCFH)	28.6	26.65
PRIMARY AIR/SECONDARY AIR VOLUMETRIC FLOW RATIO	5.2%	5.6%
GAS VELOCITY (m/s)	0.5	0.5
REYNOLDS NUMBER (Re)	147	129

Calcination tests were conducted on the Linden Hall, Bossardville, and Nittany limestones. The three sorbents have been sized into the following size fractions: 270 x 400, 200 x 270, and 140 x 200 mesh (i.e., 37-53 μm with a d_{50}

of 45 μm, 53-74 μm with a d_{50} of 63 μm and 74-105 μm with a d_{50} of 80 μm, respectively). Each size fraction will be calcined in the EFR to determine the effect of size on the extent to which particles calcine under given time/temperature conditions. The tests will be conducted at 1000 and 1100°C (reactor temperature). Samples will be extracted at different locations within the EFR to determine the effect of residence time on the extent to which each sorbent calcines. Theoretically, acoustics should not affect the calcination rate or the extent of calcination. To verify the absence of acoustic enhancement, only selected calcination tests will be performed.

To date, calcination tests without acoustics have been conducted on the samples listed in Table 7. A duplication run was conducted on the Linden Hall, 45 μm sample at 1000°C to check the reproducibility of the calcination procedure and analysis of the calcine. Samples were collected at three locations within the reactor. The extent of calcination as a function of furnace distance is shown in Figure 25. As can be seen from the graph, the results from the two tests are almost identical.

TABLE 7:

CALCINATION TESTS COMPLETED AS OF 10/1/93

SAMPLE ID	PARTICLE SIZE d_{50} (μm)	TEMPERATURE (°C)
LINDEN HALL	89	1000
	63	1000
	45	1000
BOSSARDVILLE	89	1000
	63	1000
	45	1000
BOSSARDVILLE	89	1100
	63	1100
	45	1100
LINDEN HALL	89	1100
	63	1100
	45	1100

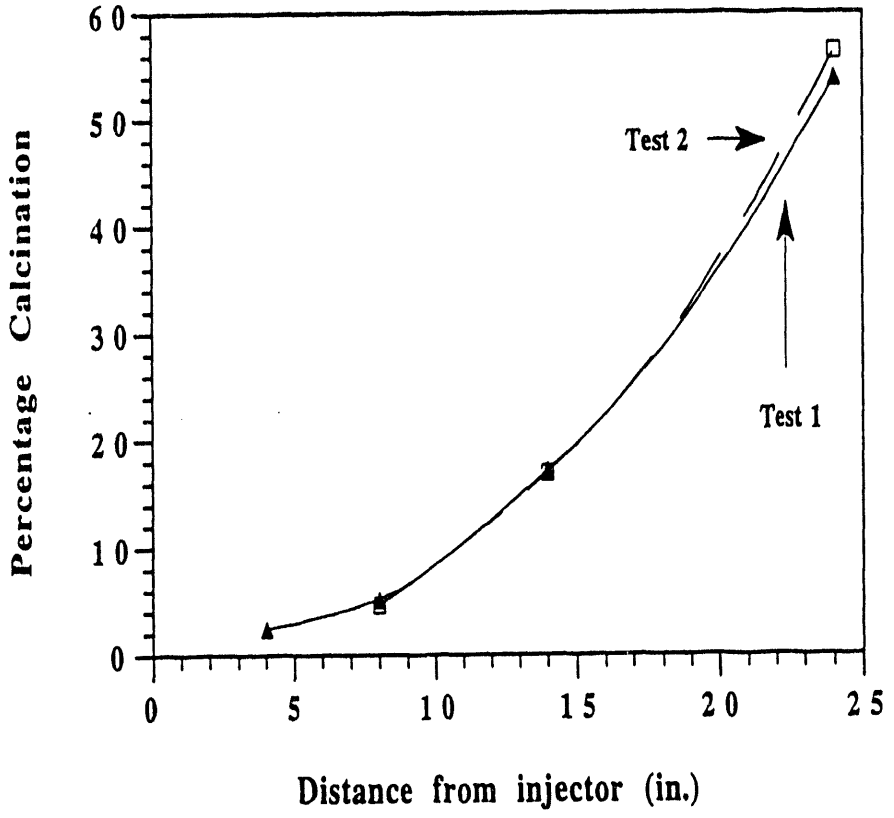

FIGURE 25: RESULTS OF DUPLICATION TESTS FOR THE LINDEN HALL, 45 μM PARTICLES AT 1000°C

The extents of calcination as a function of distance along the reactor (i.e., residence time) and particle size for the Linden Hall and Bossardville stones at 1000 and 1100°C are shown in Figures 26 through 30. The extent of calcination at any given point in the reactor for all three particle sizes increased when the reactor temperature was increased from 1000 to 1100°C. The percentage increase in calcination due to increased reactor temperature for the various samples is shown in Table 8. The increase in the extent of calcination of the Linden Hall particles increases with particle size. The Bossardville samples show no such relationship. An explanation for this behavior cannot be given until further testing is completed.

Measurement of the surface area and pore size distribution of selected calcine samples have been completed and the data are listed in Table 9. As the extent of calcination increases the surface area and total pore volume increase as shown in the Linden Hall, 45 μm, 1100°C and Bossardville, 45 μm, 1100°C samples. This is consistent with studies conducted at Penn State that show a significant increase in sorbent surface area and pore volume with the extent of calcination (Morrison, et. al. 1993). This is due to structural changes that occur during calcination accompanying the release of carbon dioxide from calcium carbonate.

The results of the baseline agglomeration tests are being compiled. No additional work will be conducted on Task 2 until the calcination and sulfation tests in Task 1 have been completed.

Theoretical modeling of the relationship of sound frequency, particle size, and the rate of convective heat transfer due to acoustics was conducted. Results will be discussed in the report for the next period.

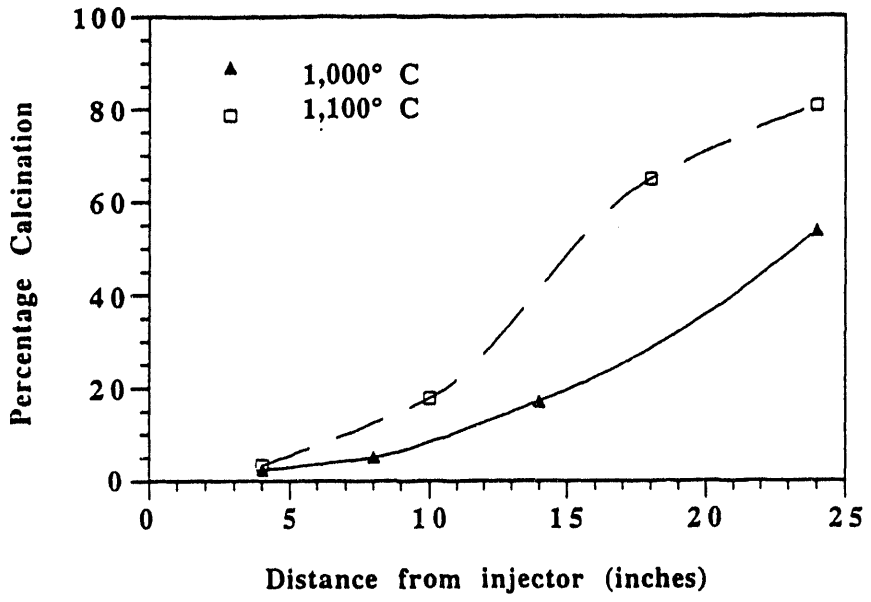

FIGURE 26: CALCINATION TEST FOR THE LINDEN HALL, 45 μM PARTICLES

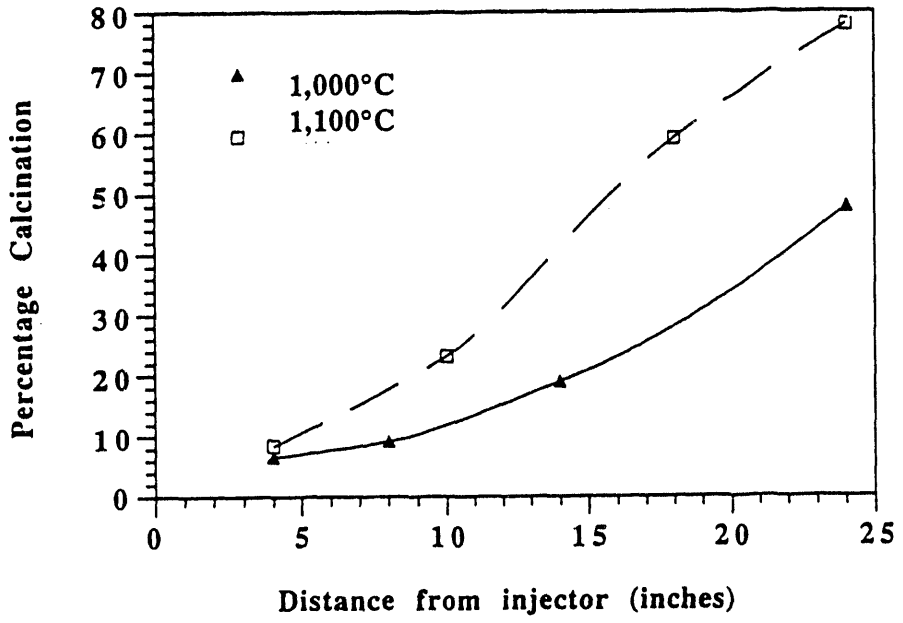

FIGURE 27: CALCINATION TEST FOR THE LINDEN HALL, 63 μM PARTICLES

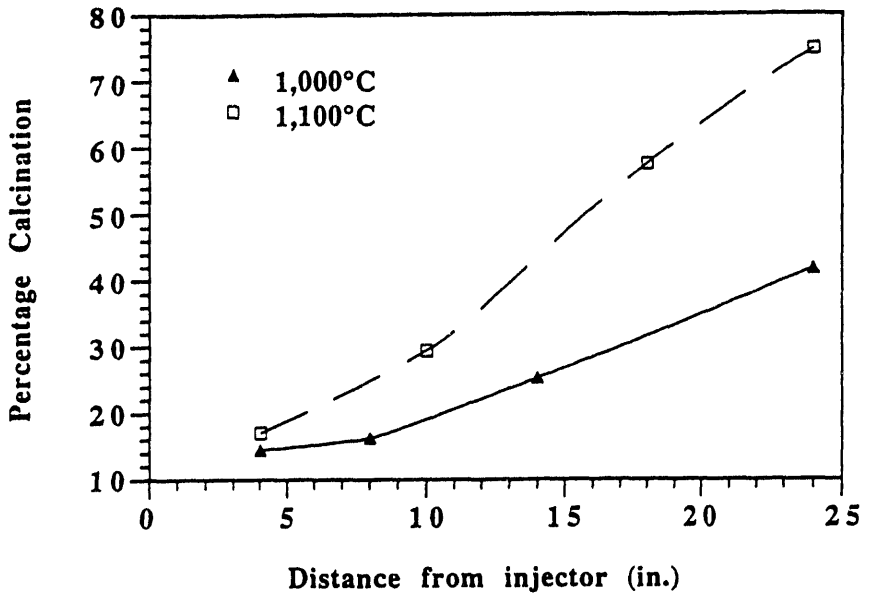

FIGURE 28: CALCINATION TEST FOR THE LINDEN HALL, 89 μM PARTICLES

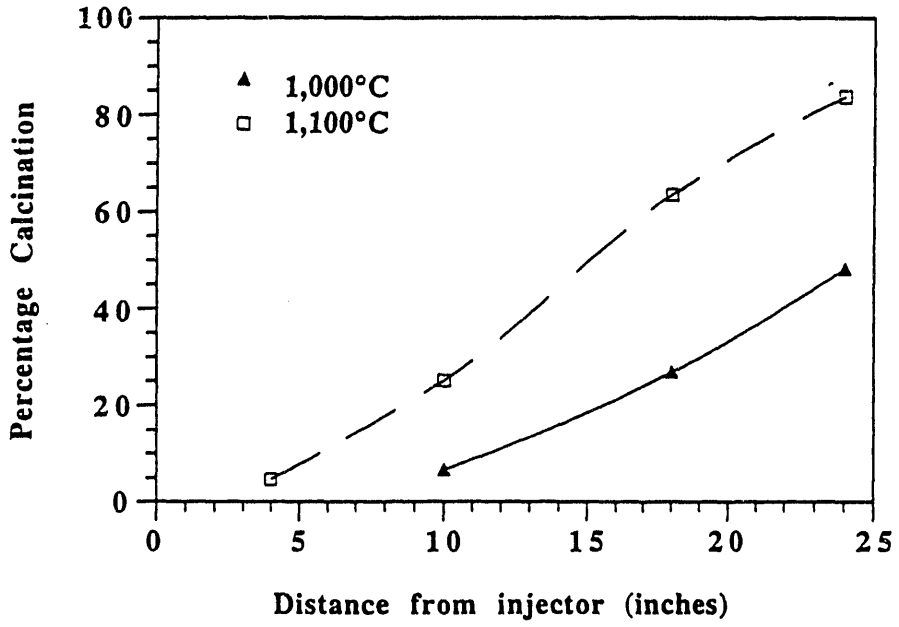

FIGURE 29: CALCINATION TEST FOR THE BOSSARDVILLE, 63 μM PARTICLES

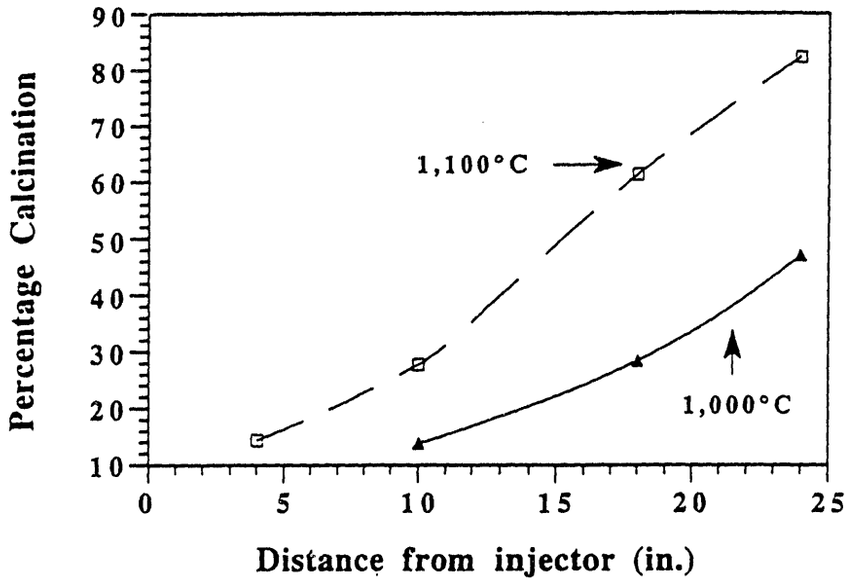

FIGURE 30: CALCINATION TEST FOR THE BOSSARDVILLE, 89 μM PARTICLES

TABLE 8:

EXTENT OF CALCINATION OF SELECTED SORBENTS AT DIFFERENT REACTOR TEMPERATURES

SAMPLE	SIZE (μm)	CALCINATION % REACTOR TEMP. (°C) 1000	1100	INCREASE IN CALCINATION (%)
LINDEN HALL	45	53.9	80.8	50
	63	47.9	77.9	63
	89	41.8	74.9	79
BOSSARDVILLE	63	48.4	83.8	73
	89	47.1	82.3	75

TABLE 9:

CALCINE SURFACE AREA AND PORE SIZE DISTRIBUTION MEASUREMENTS

SAMPLE ID, SIZE, TEMPERATURE	DISTANCE (in.) FROM INJECTOR	SURFACE AREA (m2/g)	PORE SIZE (Mode, Å)	PORE SIZE (Mean, Å)	TOTAL PORE VOLUME (cc/g)
LINDEN HALL, 45 μm, 1000°C	24	30.25	<50	78	0.0594
LINDEN HALL, 45 μm, 1100°C	10	4.49	<50	137	0.0154
	18	39.58	<50	98.5	0.0976
	24	46.72	52	99.5	0.116
BOSSARDVILLE, 45 μm, 1000°C	24	23.63	<50	91.2	0.0538
BOSSARDVILLE, 45 μm, 1100°C	10	5.75	<50	99	0.0193
	18	31.1	<50	96.5	0.075
	24	35.5	65	126	0.112

2.3.2 FUNDAMENTAL STUDY OF BIMODAL ACOUSTIC AGGLOMERATION

The PCSV-P was sent back to Insitec for repairs. Since the PCSV-P was unavailable and the preparation of the calcine by MTCI was delayed, modification and upgrading of the EFR was started. The unit was dismantled. The unit controls will be upgraded and a new collection probe will be constructed.

CALIBRATION OF PCSV-P

PCSV-P was calibrated at the Combustion Laboratory using transparent discs etched in an opaque reticle. The diameters of these transparent discs were in the range of 2.0 μm - 8.0 μm. A series of test runs were conducted to measure particle concentrations and particle size distributions of ash particles in the presence and absence of an acoustic field within the entrained flow reactor. The test matrix of the experiments was as follows:

SOUND LEVELS (dB)	FREQUENCY (Hz)
140	440
140	800
140	1000
150	440
150	800
150	1000

A number of variations in the particle concentrations and size distributions were observed with changes in sound frequency and pressure levels. The changes were attributed to the interaction of the acoustic field with the ash particles. The data generated by the experiments needs to be further analyzed to establish

whether statistically significant agglomeration of the ash particles is occurring due to the acoustic field.

2.3.3 Sulfur Capture Model

The introduction of a sulfation model into PCGC-2 has been completed. The model simulates calcination and sintering occurring concurrently with sulfation. Calcination is modeled using the classical shrinking core model. The reaction of calcination is as follows:

$$CaCO_3 \longrightarrow CaO + CO_2$$

The carbonate rate equation is obtained empirically from published thermodynamic data. The structure of CaO is represented by overlapping spheres. The rate of volume change of the particle is proportional to the surface area of the unreacted spherical core. The sintering model is simulated by overlapping of the grains by moving the grain centers closer together, thereby reducing the surface area and porosity. Qualitative results of the model indicate that the time for complete calcination for a 13 μm particle is approximately 0.3s (Figures 31 and 32). However, with increasing temperature, the surface area decreases due to sintering. In Figure 33 the relation of surface area and extent of calcination as a function of time is given for a calcium carbonate particle 13 μm in diameter, 100 m^2/g surface area, and porosity of 0.54. Just prior to complete calcination (at approximately 0.25s the surface area of the particle begins to decrease due to sintering. The surface area continues to decrease with time after calcination is completed.

The sulfation model is based on the reaction as follows:

$$S + O_2 \longrightarrow SO_2 \text{ (Gas Phase Product of Combustion)}$$
$$CaO + SO_2 + {}^1/_2O_2 \longrightarrow CasSO_4$$

The sulfation of the exposed CaO surface is assumed to be instantaneous and limited only by gas phase diffusion of SO_2 to the particle. The concentration of SO_2 is assumed to be constant and the particle stationary. Sulfur dioxide reacts with CaO to form $CaSO_4$ on the particle surface. Pore diffusion and

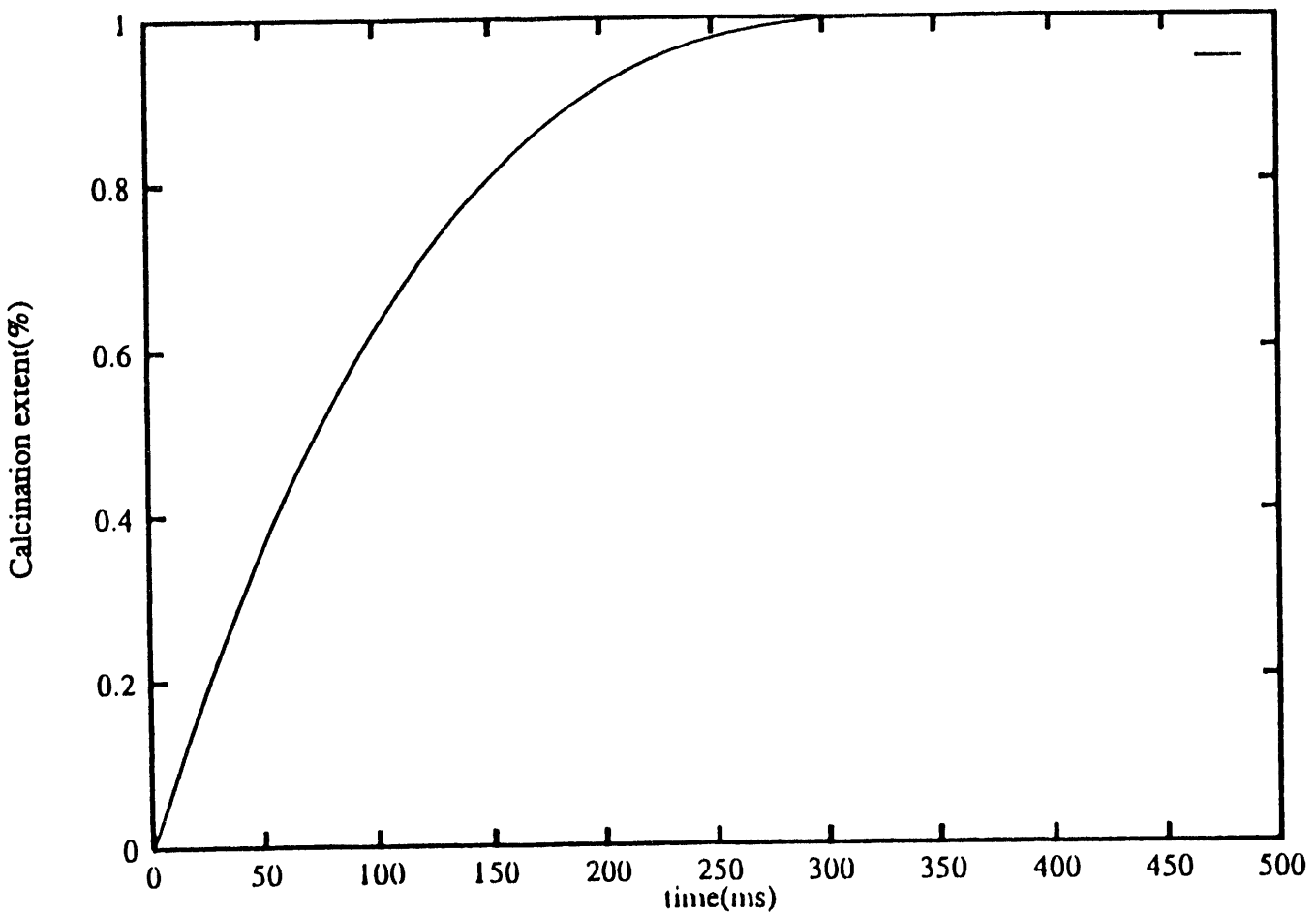

FIGURE 31: MODEL PREDICTIONS FOR 13 μM $CaCO_3$ AT 1373K

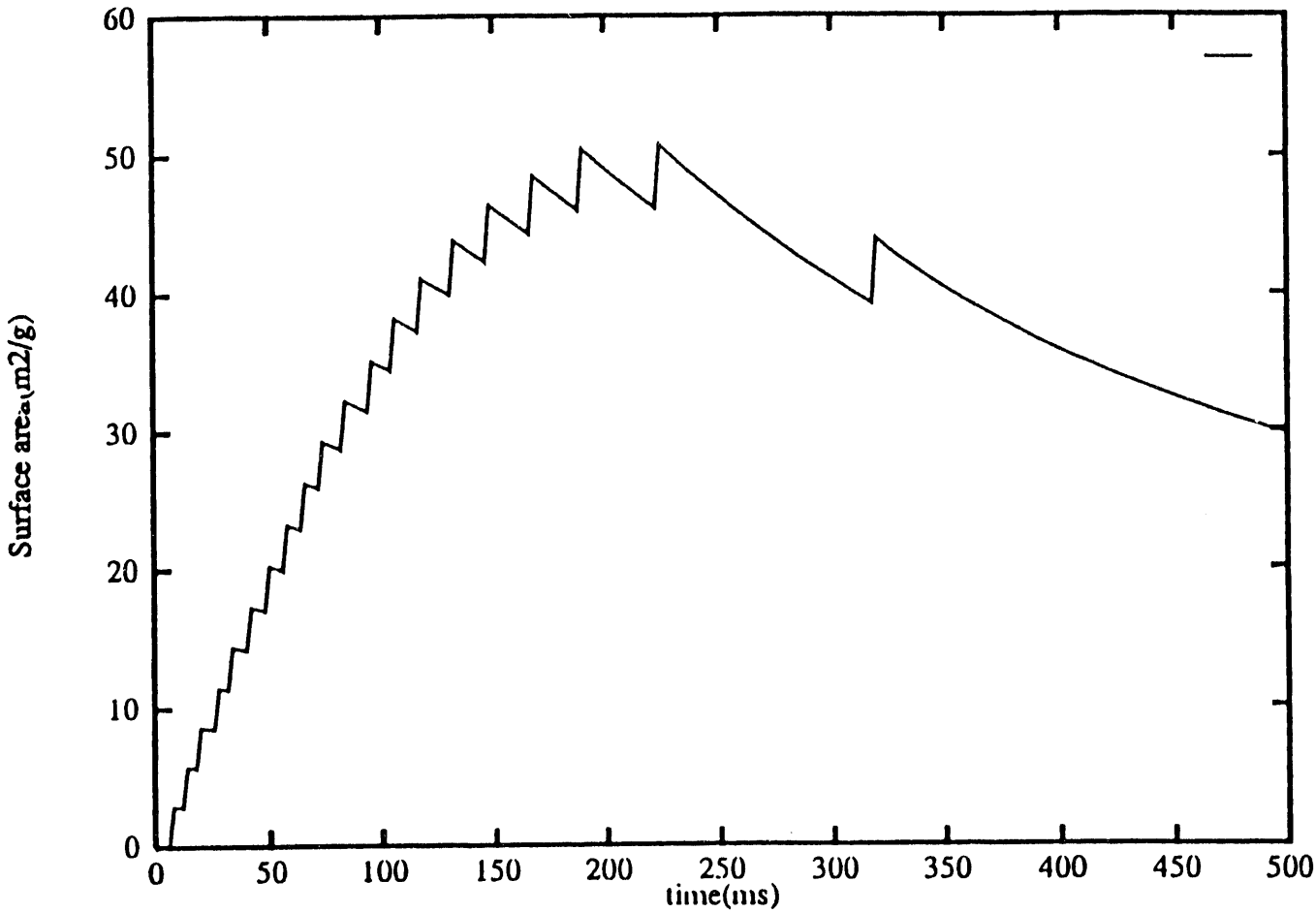

FIGURE 32: MODEL PREDICTIONS FOR 13 μM $CaCO_3$ AT 1373

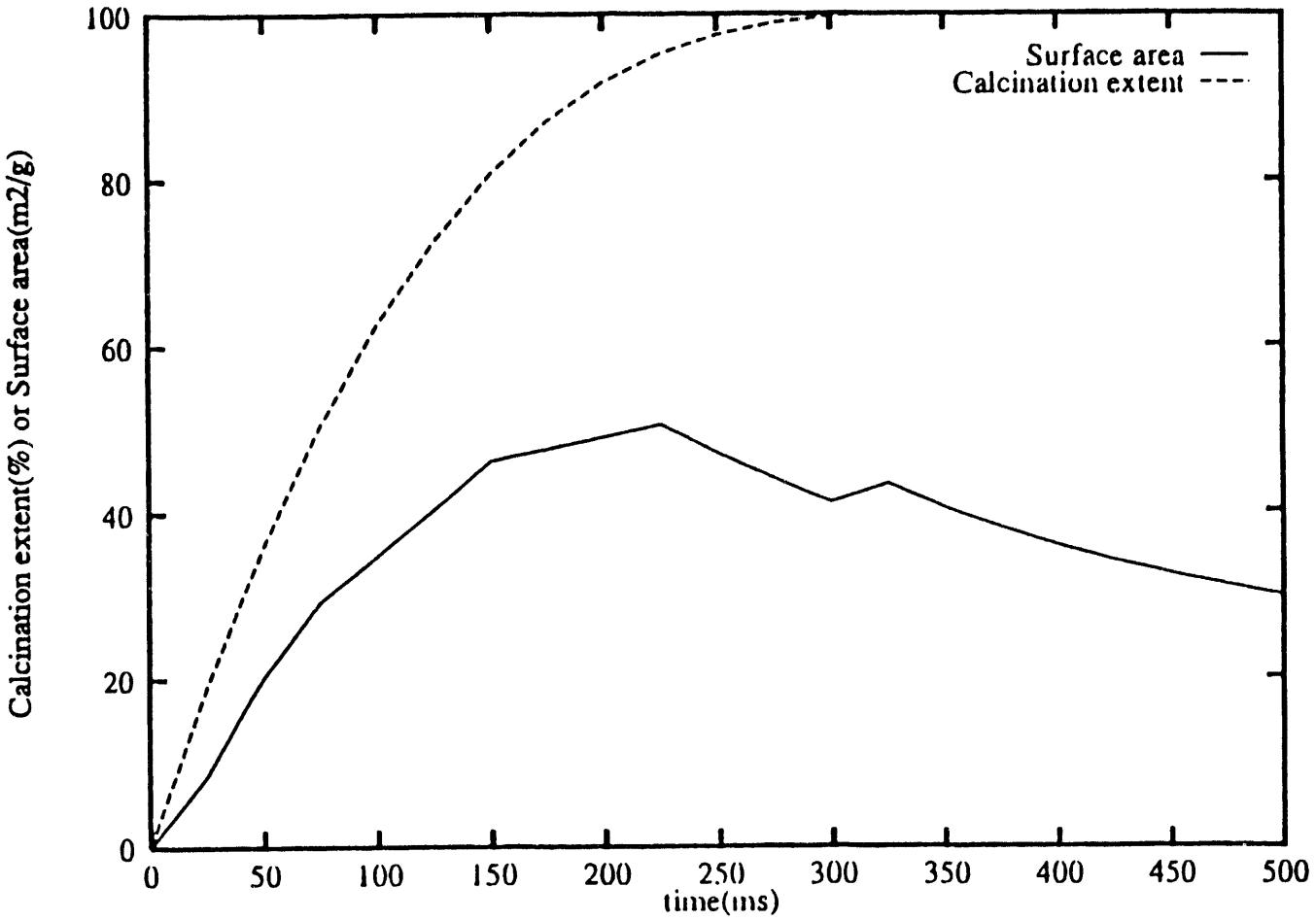

FIGURE 33: MODEL PREDICTIONS FOR 13 μM $CaCO_3$ AT 1373K, 100 M2/G, POROSITY = 0.54

product layer diffusion effects become important once a monolayer of $CaSO_4$ forms on the particle surface. The reaction rate of sulfation is assumed to be independent of the O_2 concentration.

The following observations were made modeling the sulfation of precalcinated CaO:

- Effect of Surface Area: Increasing surface area shows an increase in the extent of sulfation (Figures 34a and 34b).

- Effect of Temperature: Optimum sulfation temperature was observed at 1,364 K (Figure 35). Temperatures above and below 1,364 K showed reduced levels of sulfur capture. Significant sintering occurs at elevated temperatures, thereby reducing the reactive surface area of the calcine.

- Effect of Particle Size: Increasing particle size results in a decrease in the rate of SO_2 capture (Figure 36). This is particularly true in the initial stage of capture when pore diffusion is predominant. After 25 ms product layer diffusion is dominant and the rate of SO_2 capture decreases for all particle sizes. In addition, 7.1 and 4.1 μm in size displayed similar SO_2 capture profiles. This suggests that there is a threshold diameter below which there is little effect of particle size on SO_2 capture.

Sulfation of carbonate ($CaCO_3$) and calcium hydroxide ($Ca(OH)_2$) particles were simulated using the sulfation model and the following observations were made:

- Effect of Particle Size: Larger calcium hydroxide and carbonate particles display lower SO_2 conversion at a given time than smaller particles (Figures 37a and 37b). In addition, the initial sulfation rate is seen to be strongly dependent on particle size. The extent of SO_2 conversion at a given time for calcium hydroxide particles less

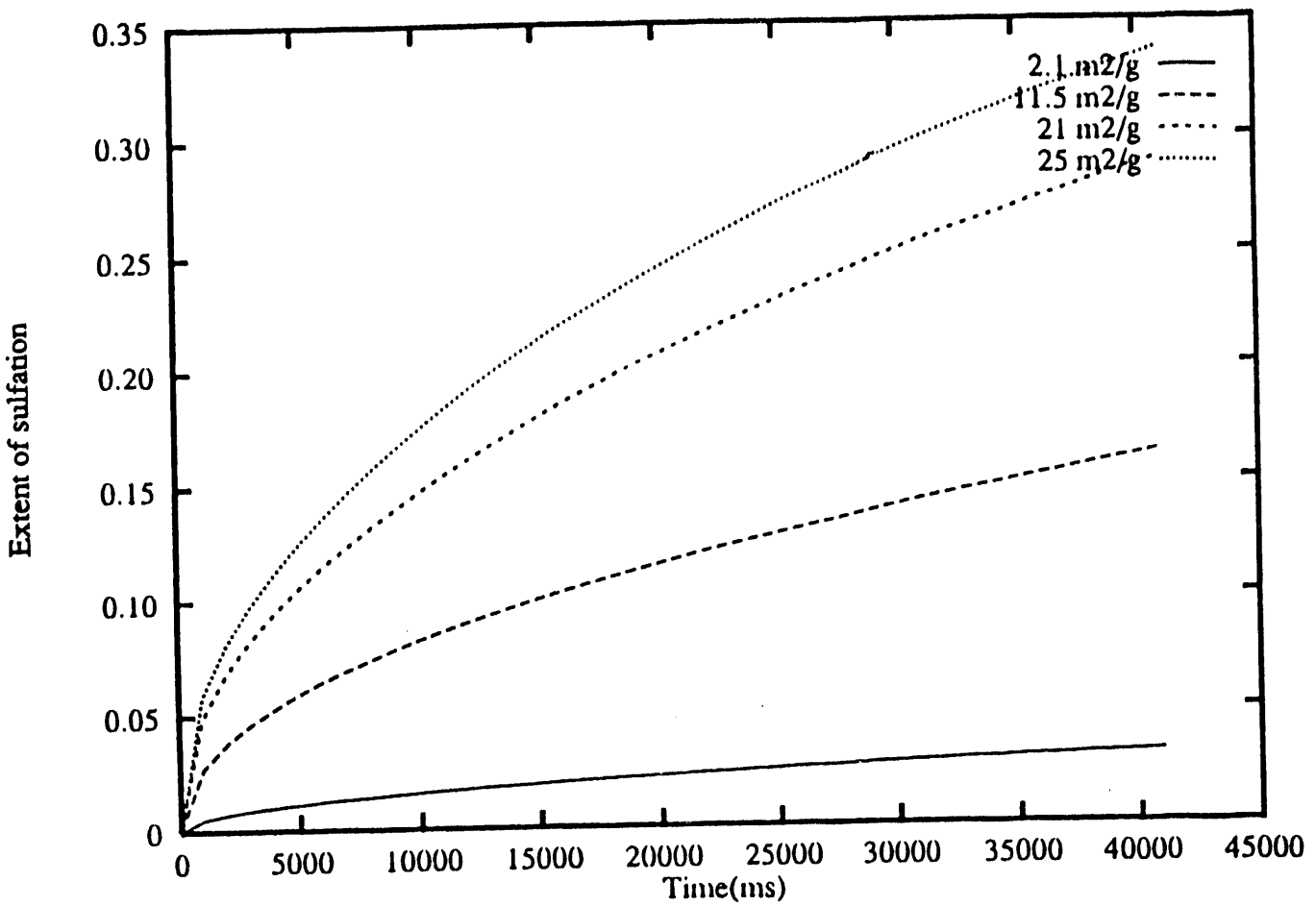

FIGURE 34A: SURFACE AREA EFFECTS: 1 μM CaO, 304 Pa SO_2, 1073K

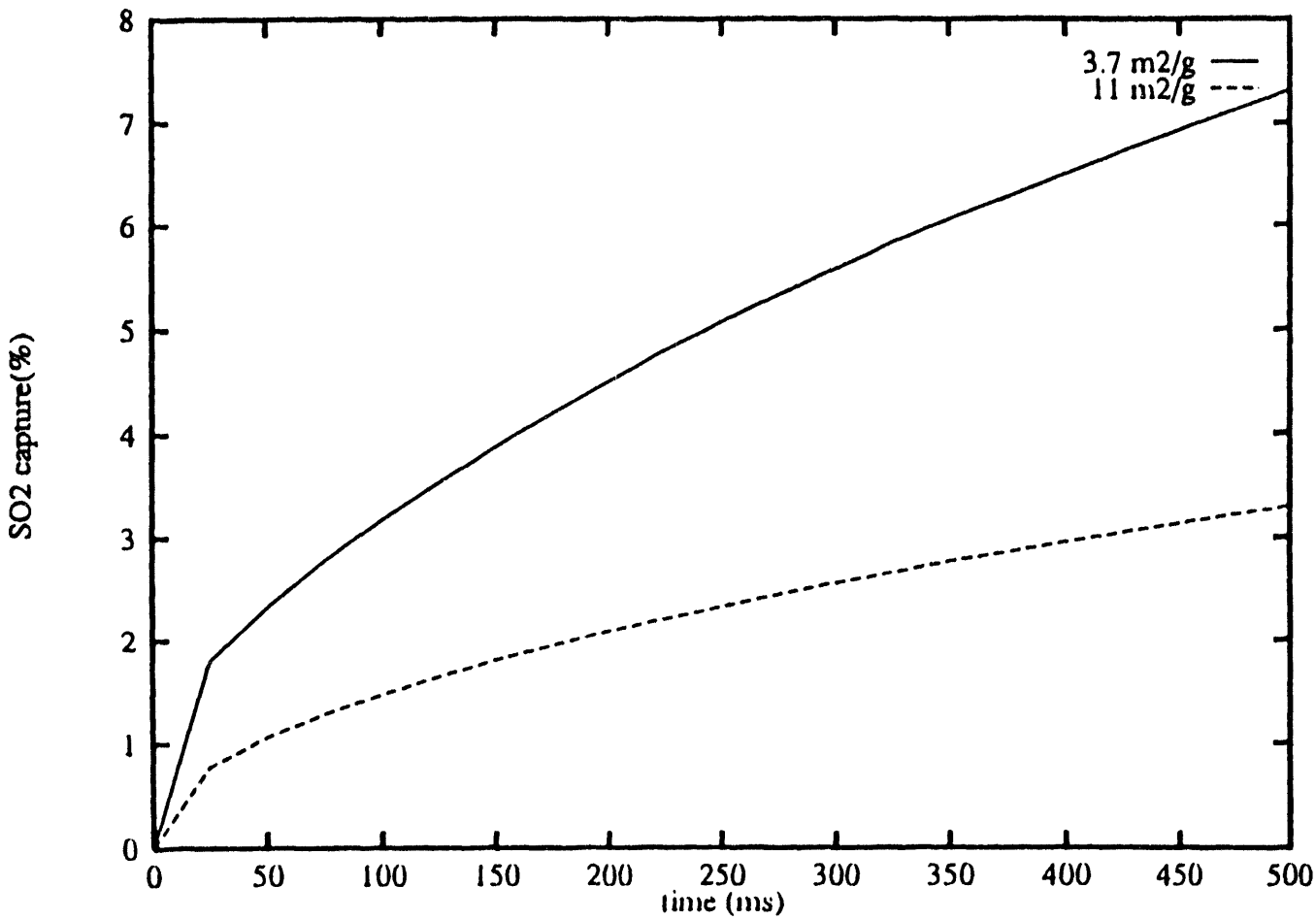

FIGURE 34B: SULFATION OF 7 μM C-CaO, 148 PA, 1367K, POROSITY = 0.15

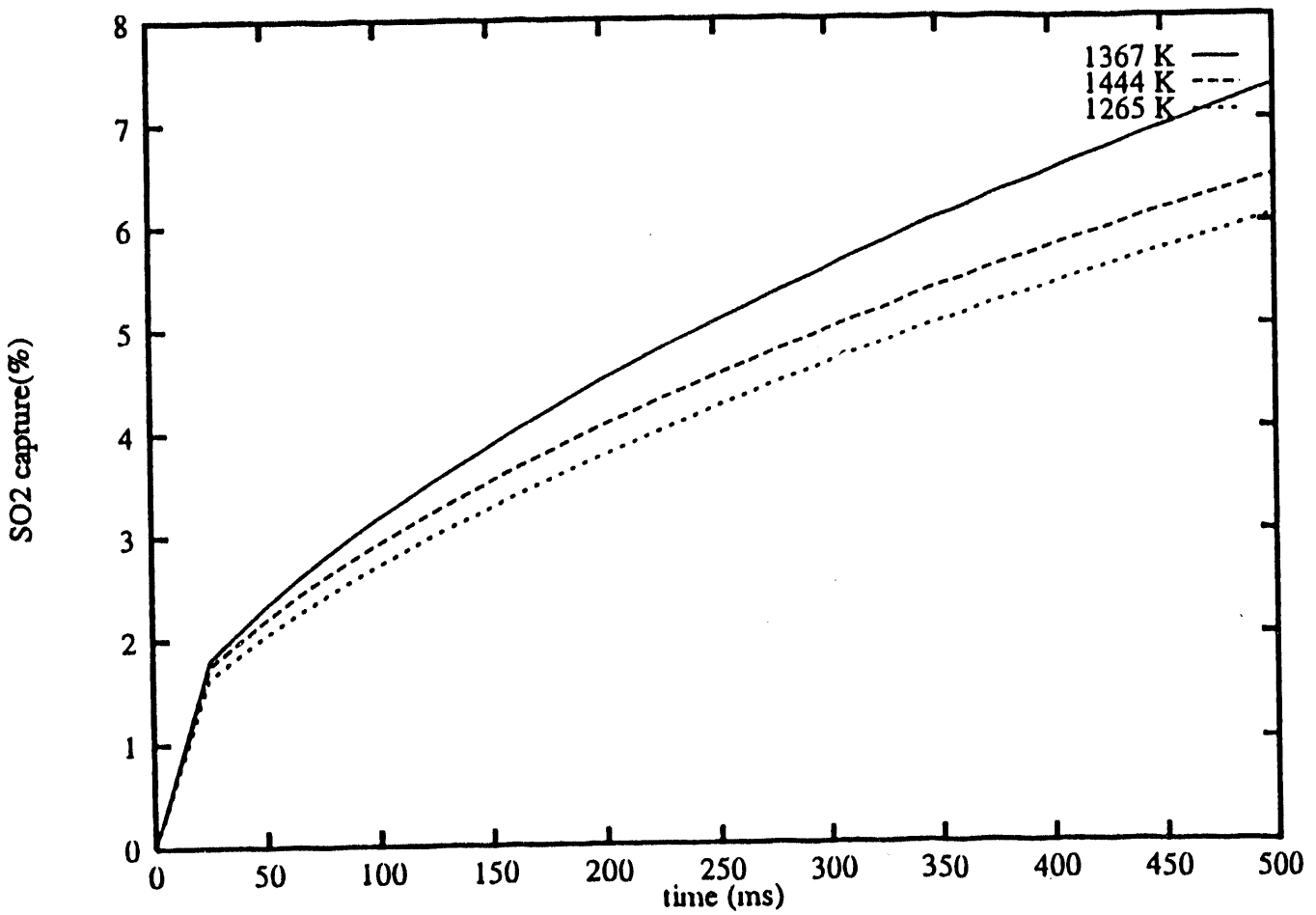

FIGURE 35: SULFATION OF 7 μM C-CaO - INFLUENCE OF TEMPERATURE, 11 M2/G

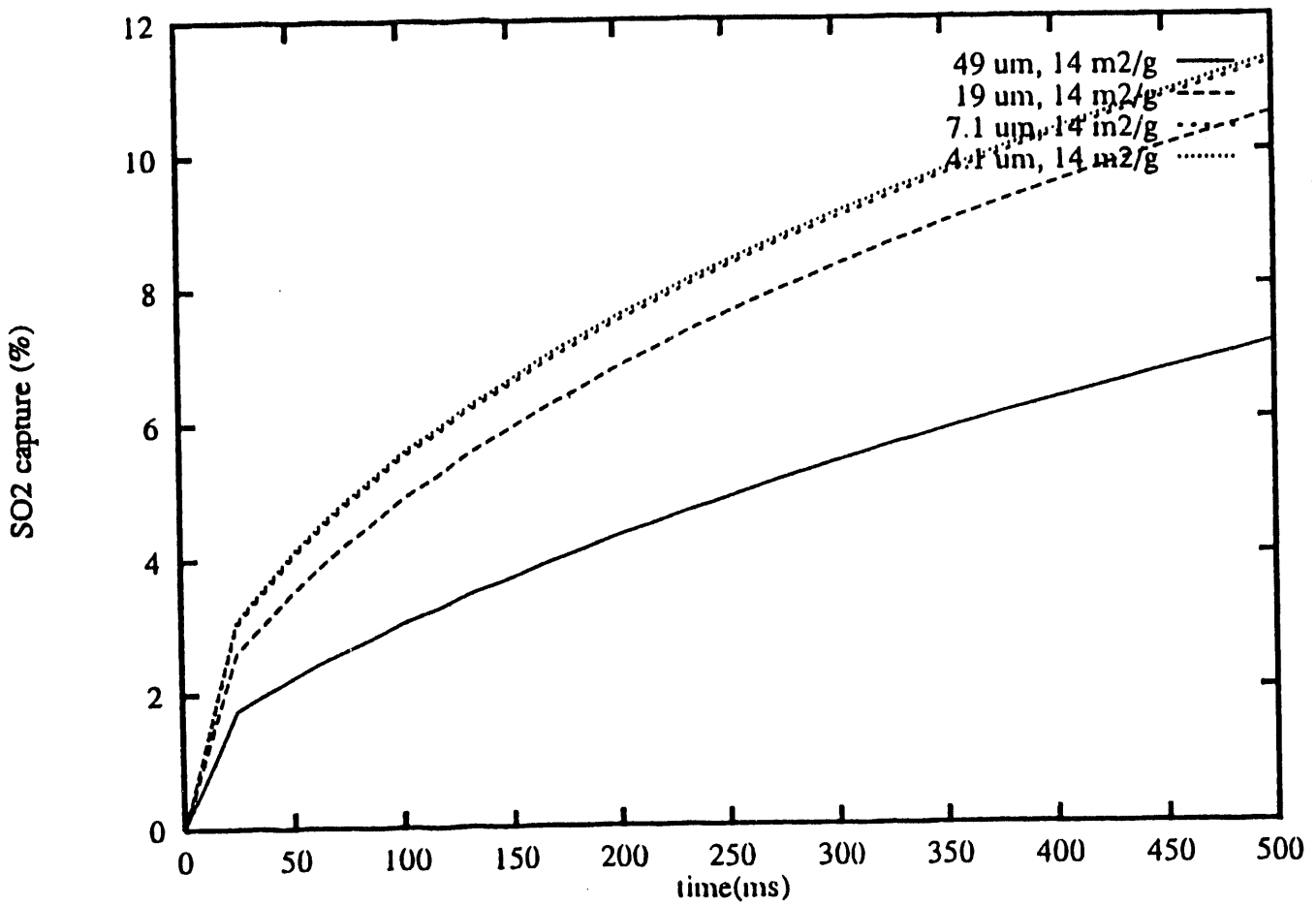

FIGURE 36: PARTICLE SIZE EFFECT ON SULFATION OF C-CaO

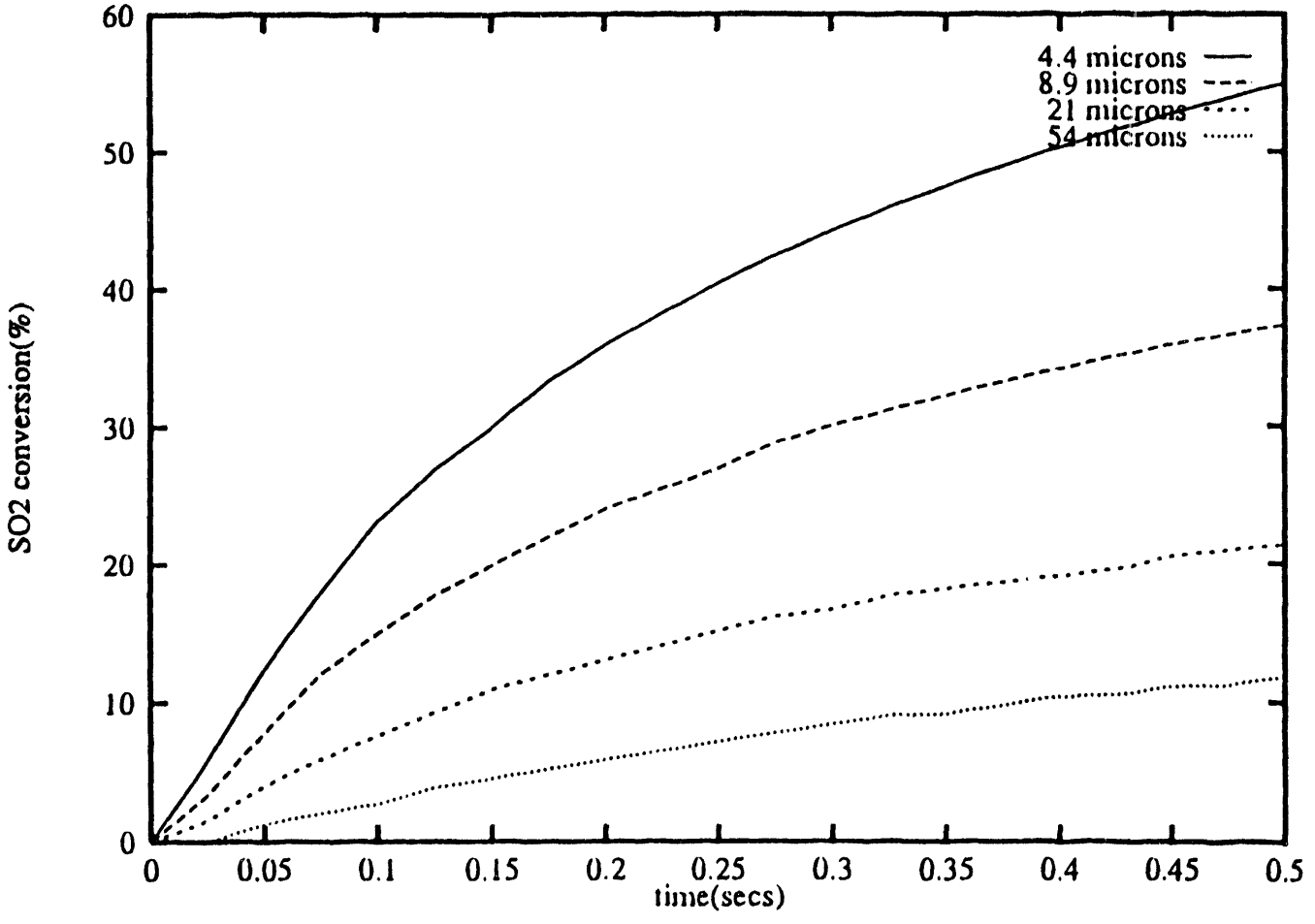

FIGURE 37A: PARTICLE SIZE INFLUENCE, LINWOOD CARBONATE, 1367K, 148 PA SO_2

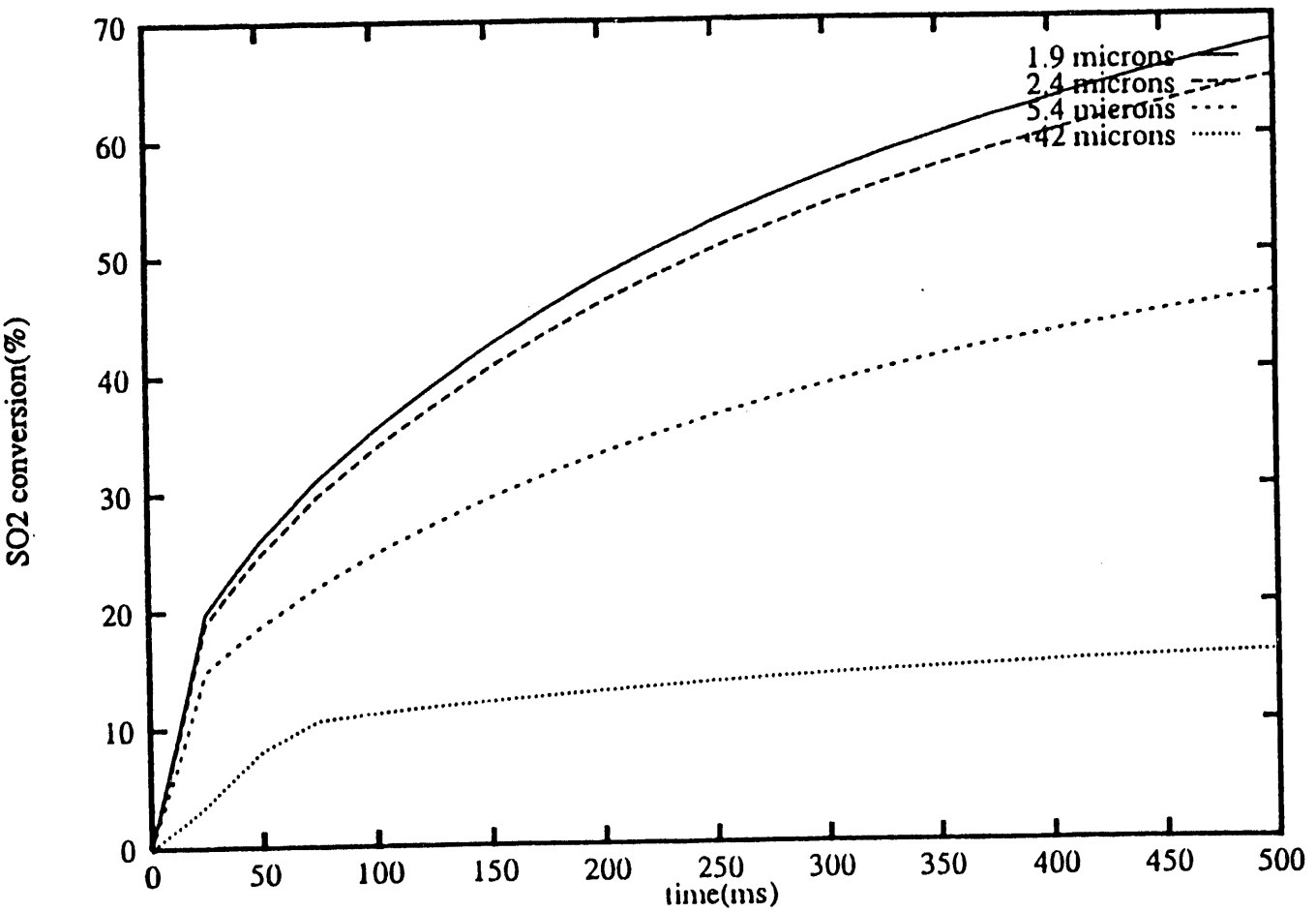

FIGURE 37B: PARTICLE SIZE INFLUENCE, LINWOOD HYDRATE, 1367K, 148 PA SO_2

than 2.4 μm is independent of particle size. The rate of sulfur capture decreases for the calcium hydroxide particle after 25 ms for smaller particles, i.e., ≤ 5.4 μm. The rate of sulfur capture decreases for the calcium hydroxide particle after 75 ms for larger particles, i.e., 42 μm.

The rate of SO_2 conversion for the carbonate particles is a function of particle size (Figure 37a). Sulfur dioxide conversion at a given time is dependent upon particle size even down to 4.4 μm. The rate of SO_2 conversion decreases with time as sulfation proceeds. Particle size effects are produced by pore-diffusion limitations in larger particles since pore diffusivity is a function of particle radius.

- Rate and Extent of SO_2 Capture: The rate of calcination and sulfation for a calcium hydroxide particle was much higher than that of a similar size carbonate particle (Figure 38). Therefore, $CaSO_4$ product layer forms on the calcium hydroxide particle very early, thereby limiting diffusion of SO_2 into the particle. In addition, the calcium hydroxide particles were predicted to sinter to a greater extent than the carbonate particles, thereby reducing the active surface layer in the calcium hydroxide to a greater extent than in the carbonate. Therefore, a carbonate particle reacts with SO_2 at a higher rate after 25 ms than a calcium hydroxide particle. The result is that the extent of SO_2 conversion of carbonate particles is greater than that of calcium hydrate particles.
- Effect of Temperature: SO_2 conversion is influenced by temperature (Figure 39). The optimum temperature for sulfation was 1,364 K. While product layer diffusivity increases with temperature so does the occurrence of sintering. The effect of sintering of the particle surface is a reduction in the reactive surface area.
- Effect of Sintering: Sintering of $CaCO_3$ particles is shown to decrease the extent of SO_2 conversion (Figure 40). Sintering of the particle surface reduces the effect of diffusion of SO_2 to reactive pore surfaces.

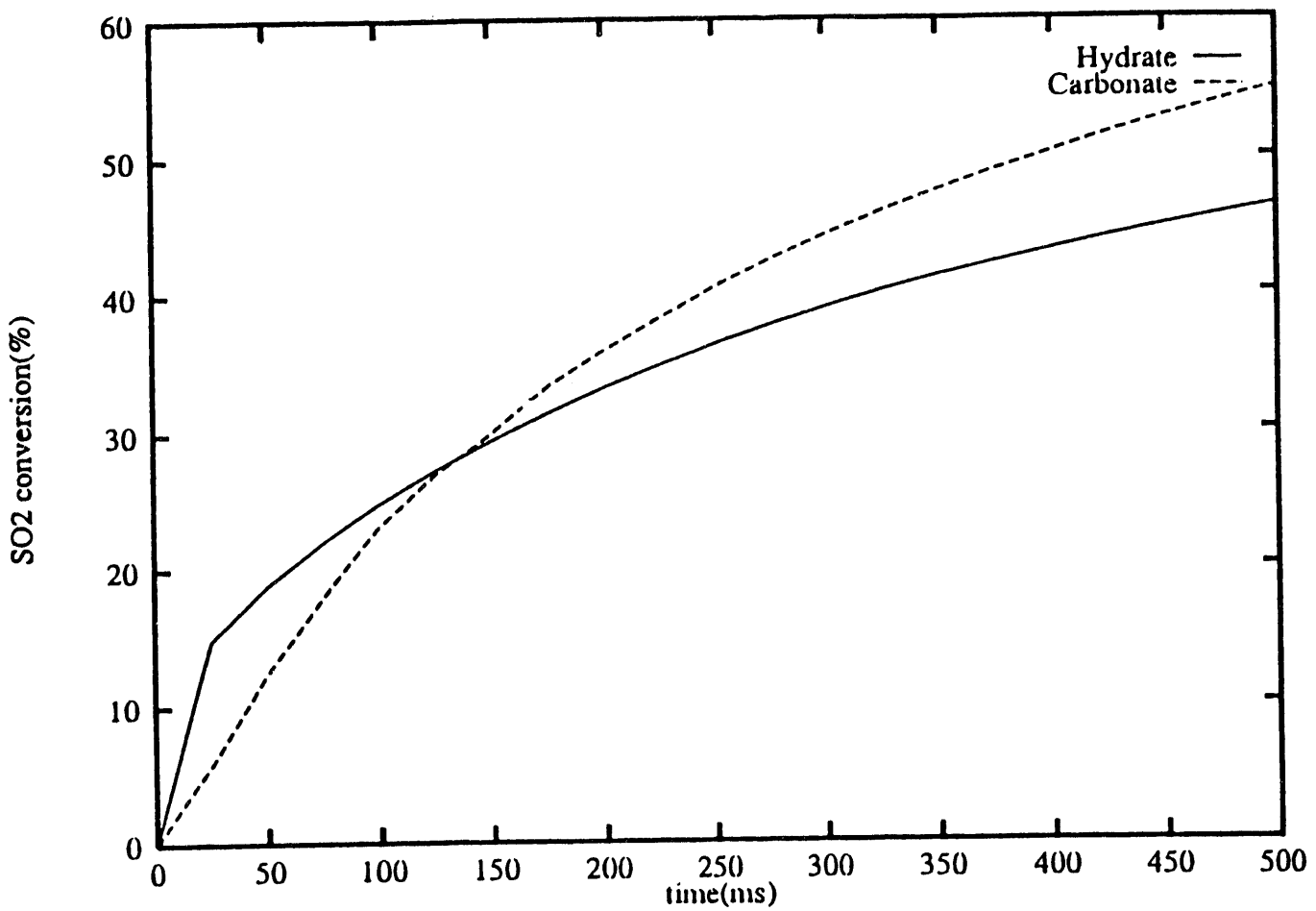

FIGURE 38: COMPARISON OF HYDRATE (5.4 μM) AND CARBONATE (4.4 μM), 1367K, 148 PA SO_2

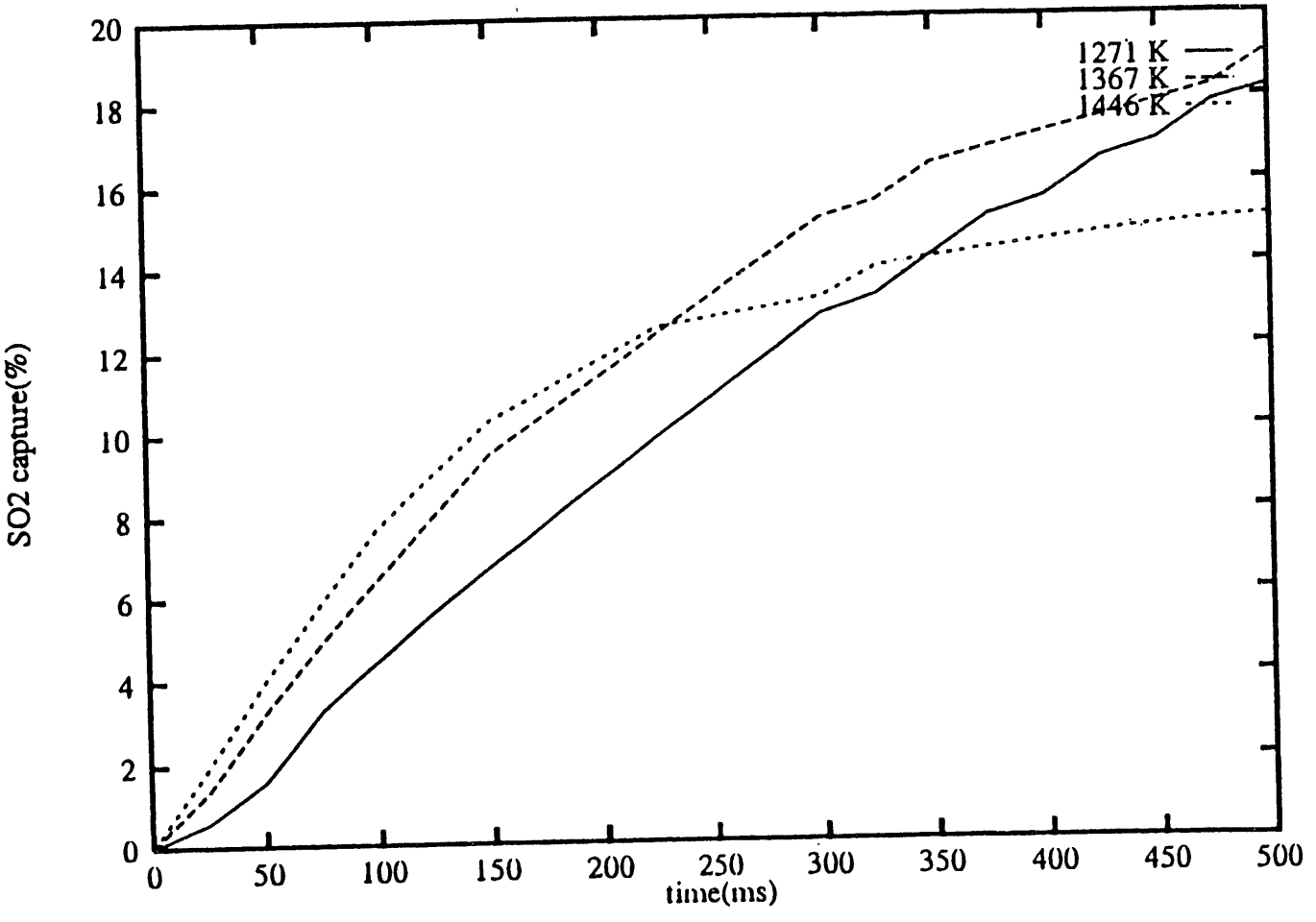

FIGURE 39: TEMPERATURE INFLUENCE, 25 μM LINDWOOD CARBONATE

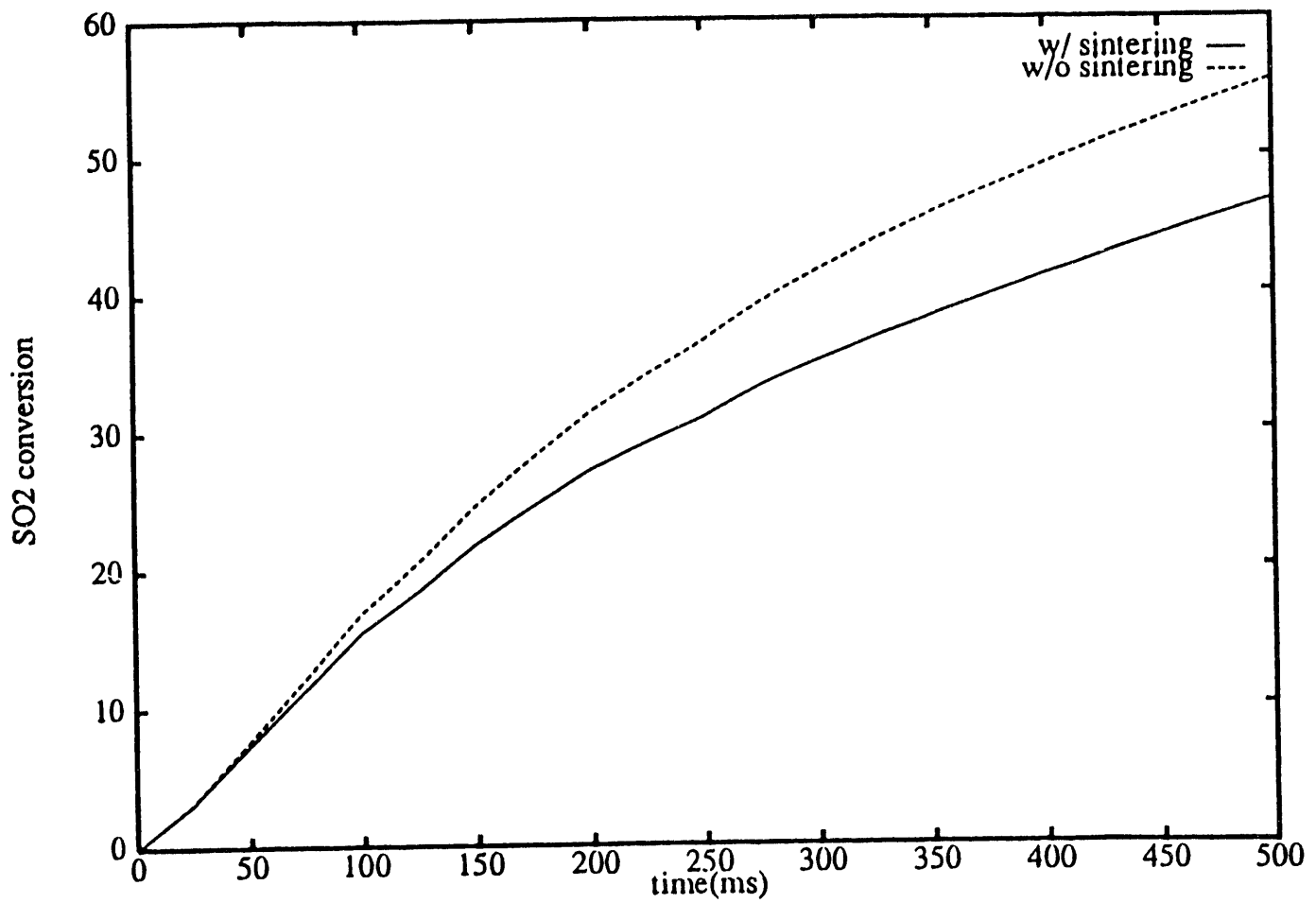

FIGURE 40: SINTERING INFLUENCE ON 10 μM CaCO3

These observations will be compared to the experimental observations from the calcination and sulfation tests conducted in the EFR (Task 1).

SECTION 3.0

PLANS FOR NEXT PERIOD

- Testing will be initiated during the next period.
- WVU - In the coming weeks an optimization of the diffuser-length-to-throat-width ratio will be performed and a test valve will be constructed to verify the design analysis.
- PSU - During the next period, sulfation tests will be initiated and work on the model will proceed.

DATE
FILMED
3/7/94
END